Title: Temporal pattern and synergy influence activity of ERK signaling pathways during L-LTP induction

Authors:

1. Nadiatou T. Miningou Zobon
   Department of Chemistry and Biochemistry, George Mason University, Fairfax, VA 22030, USA
2. Joanna Jędrzejewska-Szmek
   Laboratory of Neuroinformatic, Nencki Institute of Experimental Biology of Polish Academy of Sciences, Warsaw, Poland
3. Kim T. Blackwell
   Interdisciplinary Program in Neuroscience, Bioengineering Department, and Krasnow Institute for Advanced Study, George Mason University, Fairfax, VA 22030, USA

Corresponding Author: Kim T. Blackwell, Krasnow Institute for Advance Study and Department of Bioengineering, MS 2A1, George Mason University, 4400 University Drive, Fairfax, VA, 22030, USA

Conflict of Interest: The authors declare no competing financial interests.

Acknowledgments: This work was supported through the joint NIH-NSF CRCNS program through NSF grant 1515686 and NIMH grant R01MH 117964

Competing interests: The authors declare no competing interests

ABSTRACT

Long-lasting long-term potentiation (L-LTP) is a cellular mechanism of learning and memory storage. Studies have demonstrated a requirement for extracellular signal-regulated kinase (ERK) activation in L-LTP produced by a diversity of temporal stimulation patterns. Multiple signaling pathways converge to activate ERK, with different pathways being required for different stimulation patterns. To answer whether and how different temporal patterns select different signaling pathways for ERK activation, we developed a computational model of five signaling pathways (including two novel pathways) leading to ERK activation during L-LTP induction. We show that calcium and cAMP work synergistically to activate ERK and that stimuli given with large inter-trial intervals activate more ERK than shorter intervals. Furthermore, these pathways contribute to different dynamics of ERK activation. These results suggest that signaling pathways with different temporal sensitivity facilitate ERK activation to diversity of temporal patterns.

INTRODUCTION

Temporal patterns are a key feature of the environment. The speed of traversing space is indicated by the time between spatial cues. In classical conditioning, adaptive changes in behavior require an animal to respond to a cue in an appropriate time frame to gain a reward or avoid punishment (Delamater and Holland, 2008; Mauk and Ruiz, 1992). In these and other tasks, environmental cues, i.e., sensory inputs, are converted into spatio-temporal patterns of activation. Pattern discrimination requires that neurons are able to discriminate and respond differently to these different temporal input patterns (Bhalla, 2017); conversely, neurons need to be able to learn *despite* a difference in temporal patterns.

Long-term potentiation (LTP), the activity-dependent and persistent strengthening of synapses, is widely considered to be a cellular mechanism underlying memory storage. The temporal pattern sensitivity of neurons is evident from the wide range of synaptic plasticity induction protocols, with some protocols producing LTP and some producing weakening of synapses (Malenka and Bear, 2004). Memory consolidation is also affected by temporal patterns: it has been shown that theta oscillations, which emerge during learning, and sharp-wave ripples can influence LTP induction (Çalışkan and Stork, 2018; Sadowski et al., 2016; Wang et al., 2020), demonstrating a role for temporal patterns during memory consolidation.

In the hippocampus, two “phases” of LTP are distinguished. Late phase LTP (L-LTP), induced by repetitive stimulation, can last more than 8 hours and involves de novo protein synthesis (Davis et al., 2000; Sweatt, 2004; Tang and Yasuda, 2017). In contrast, early-phase LTP does not require protein synthesis, and typically does not persist for more than 2 hours. It is also important to distinguish between induction and maintenance of L-LTP. Induction of L-LTP

refers to the processes occurring during and shortly after the induction stimulation, whereas maintenance of L-LTP refers to the processes occurring tens of minutes to hours after induction.

A critical molecule in induction of L-LTP and memory is extracellular signal-regulated kinase (ERK) (English and Sweatt, 1997). Numerous studies have demonstrated that ERK contributes to L-LTP induction by controlling the transcription and protein translation necessary for L-LTP (for review Miningou and Blackwell, 2020; Peng et al., 2010), as well as increasing cell excitability by phosphorylating potassium channels (Schrader et al., 2006). ERK is activated by a cascade of kinases (Buscà et al., 2016; Terrell and Morrison, 2019), which are activated by Ras family GTP binding proteins, which are controlled by diverse Guanine nucleotide Exchange Factors (GEFs) and GTPase Activating Proteins (GAPs). Several of these GEFs and GAPs play a pivotal role in synaptic plasticity and neurodevelopmental disorders, but their role in ERK activation during induction of L-LTP has not been demonstrated.

In the hippocampus, synaptic stimulation leads to activation of these GEFs and GAPs. Influx of calcium activates the calcium-sensitive GEF, RasGRF (Feig, 2011; Schwechter et al., 2013), and, via CaMKII, enhances activity of the synaptically localized GAP, SynGap, while dispersing it from the spine (Gamache et al., 2020). The intracellular second messenger Cyclic Adenosine MonoPhosphate (cAMP) activates two key molecules upstream of ERK activation: protein kinase A (PKA) and the GEF exchange factor activated by cAMP (Epac)(de Rooij et al., 2000; Enserink et al., 2002; Schmitt and Stork, 2002). However, the contribution of calcium and cAMP pathways to ERK activation during L-LTP induction is unclear. A critical question is to what extent those signaling pathways work synergistically to activate ERK, whether they are redundant, or whether they operate in different temporal regions.

A second critical question is how patterns of synaptic input determine which set of signaling pathways activate ERK leading to the induction of L-LTP. Key ERK activators, such as PKA and CaMKII, exhibit different temporal sensitivity: cAMP/PKA favors spaced LTP stimulation protocols (Kim et al., 2010; Scharf et al., 2002; Woo et al., 2003) while calcium/CaMKII prefers massed LTP stimulation (Ajay and Bhalla, 2004; Kim et al., 2010). Both of these signaling pathways converge on ERK, allowing the neuron to learn despite a variation in temporal pattern; on the other hand, temporal pattern can still influence the response of the neuron by controlling the temporal pattern of ERK activation. For example, transient ERK, leads to proliferation, while sustained ERK, leads to differentiation (Santos et al., 2007; Sasagawa et al., 2005; von Kriegsheim et al., 2009).

To answer these questions about temporal pattern and synergy, we developed a single compartment computational biochemical model of postsynaptic signaling pathway underlying L-LTP induction in hippocampal CA1 pyramidal neurons. Simulations reveal that ERK pathways work synergistically, that the contribution of cAMP increases while the calcium contribution decreases with spaced stimuli, with ERK activity favoring spaced stimuli. The calcium- and cAMP-activated pathways have distinct temporal dynamics, providing a mechanism whereby different temporal patterns can activate different downstream effectors.

RESULTS

Model validation

To investigate how temporal pattern of synaptic activity determines which pathway in the ERK signaling cascade (Figure 1A, Figure 1 - Supplementary Table1&2) dominates in dendritic spines of hippocampal CA1 pyramidal neurons, we developed a single compartment, stochastic

reaction-diffusion model of pathways activating ERK. The model included two calcium signaling pathways (RasGRF and SynGap) and three cAMP signaling pathways (Epac, PKA and the βγ subunit of Gi). The model was built by merging and adapting two existing models of synaptic plasticity in hippocampal neurons (Jain and Bhalla, 2014; J□drzejewska-Szmek et al., 2017). These previously published models were modified by adding SynGap and RasGRF, which are critical for ERK activation.

To validate the model, we replicated the results from several published experiments. First, we simulated an experiment measuring RasGTP in response to glutamate uncaging at 0.5 Hz with 0 mM extracellular Mg^{2+} (Harvey et al, 2008), by delivering a single pulse of 0.5 μM of calcium for 60 sec. RasGTP dynamics are qualitatively consistent with experimental measurements of Harvey et al, 2008 (Figure 2A). Second, we mimicked an L-LTP experiment that applied two trains of 100 Hz frequency spaced by 20 sec intervals (Kasahara et al., 2001), by injecting 5 μM calcium, 1 μM cAMP, and 0.1 μM of Giβγ. The simulation shows qualitative match of ERK activation to the experimental model as ERK peaks around 3 min after stimulation and returns to basal about 30 min after stimulation (Figure 2B). Additional validations, comparing results to knockout experiment, are shown after the L-LTP results.

Single-pulse stimuli: maximal ERK activation requires multiple pathways

In order to assess if multiple pathways are required for maximal ERK activation, both single pathway and multi-pathway dynamics were monitored. Simulation experiments used different amplitude ranges (for 1 sec) and different durations of the input to evaluate doubly phosphorylated ERK (ppERK) (Table 1). We assessed whether the ERK response is graded or ultra-sensitive and whether multiple pathways combine linearly or nonlinearly.

Linear activation by cAMP pathway: Opposite dynamics of Epac and PKA

cAMP activates ERK through three different pathways: Epac activation of Rap1GTP, PKA phosphorylation of Src and PKA phosphorylation of β adrenergic receptors (βAR), which switches βAR coupling from Gs to Gi, which is followed by Giβγ recruitment of Src (Lin et al., 2013; Luttrell et al., 1997). To separate the direct action of cAMP (i.e., Epac activation of Rap1GTP or PKA phosphorylation of Src) from its indirect action through the switching pathway, we evaluated the effect of Giβγ separately and in combination with Epac and PKA direct activation.

Model simulations show a linear activation of ppERK with either cAMP duration or concentration (Figure 3, Figure 3 - Supplementary Table 3), through the direct pathway and a slightly non-linear activation with indirect pathway. As observed in Figure 3A&B, as the input duration increases, ppERK amplitude and duration increase. Similarly, the indirect cAMP pathway displays linear activation of ERK with Giβγ input (Figure 3C). Figure 3D shows that increasing the input duration (red traces) or concentration (black trace) is similarly effective in increasing ppERK. Giβγ produces a delayed activation of ERK consistent with experimental data (Koch et al., 1994; Schmitt and Stork, 2002) and a computational model showing a 7 min delay (Khalilimeybodi et al., 2018). In summary, in response to cAMP input, ppERK total activity is linearly related to the input duration and concentration, with a delayed activation through the indirect pathway.

To investigate the activation of ERK by Epac and PKA individually, the simulations were repeated while blocking cAMP binding to one of these molecules (Table 2). When cAMP binding to Epac is blocked, the basal quantity of ppERK is dramatically reduced (results not shown), implying that Epac is the main source of basal ppERK. The remaining activity, due to

PKA, shows a delayed activation of ERK (Figure 3F). In contrast, Epac produces a fast and transient activation of ERK (Figure 3F). Similarly, to PKA activation, Giβγ shows a delayed activation of ERK (Figure 3F). Thus, Epac contributes to ERK activation with different temporal dynamics compared to PKA and Giβγ.

Direct and indirect cAMP pathways combine linearly for short duration inputs and sublinearly with prolonged duration inputs. Figure 3E shows that the response to stimulating all three cAMP pathways overlaps with the sum of the single pathway responses only at a short duration. As the stimulus duration increases, the ppERK response is slightly lower than the sum of responses to cAMP direct and indirect activation (Figure 3E, Figure 3F). Sublinear summation is due to two loci of competition. First, competition was observed between the PKA phosphorylation of Src and Giβγ activation of Src. PKA has a higher affinity for Src than does Giβγ, therefore, Src is trapped by PKA, reducing available Src for Giβγ. This sublinear response is observed with 2x and 4x increases in Src quantity (results not shown) demonstrating that the sublinear summation is not due to Src depletion but indeed due to Giβγ and PKA competition with Src. The second competition was observed between Epac and the Giβγ/Crk-C3G for Rap1GDP. Rap1GDP is utilized by Epac, which reduces the Rap1GDP availability for Giβγ/Crk-C3G. Blocking Epac allows more Rap1GDP to bind Crk-C3G, prolonging ppERK activity as observed with Giβγ alone. In conclusion, competition between PKA and Giβγ for Src, and between Epac and Crk-C3G for Rap1GDP, affects summation in the cAMP pathway.

Non-linear activation by calcium pathways: SynGAP dispersion and phosphatase activity control ERK activation by calcium

Model simulations show a non-linear activation with either calcium duration or concentration. Figure 4A reveals that low calcium inputs produce little to no ppERK, whereas

with higher calcium inputs ppERK reaches a plateau and the duration of ppERK is prolonged. Similar results are observed with increasing duration using 0.5 μM calcium concentration. Total activity of ppERK (Figure 4B), reveals a supralinear response (also called ultrasensitivity), with a calcium duration threshold of 5 sec and an amplitude threshold between 1 and 2 μM. A calcium amplitude or duration above these thresholds induces maximal and sustained ppERK.

To determine if the ultrasensitivity of ppERK was caused by CaMKII, we blocked CaMKII phosphorylation (of itself and SynGap) and assessed ERK activation by RasGRF. Blocking CaMKII significantly reduces ppERK activity, especially for long or high calcium inputs (Figure 4C). We also observed a shift from a sustained and prolonged ppERK to a transient ppERK, which is caused by calmodulin activation of RasGRF (Figure 4G). This shows that RasGRF is responsible for the early calcium activation of ERK.

The ultrasensitivity of CaMKII autophosphorylation has been shown to depend on the quantity of the phosphatase PP1 (Bradshaw et al., 2003; Singh and Bhalla, 2018), and thus might regulate the calcium duration and amplitude thresholds. We used a concentration of 3.6 μM of PP1 (PP1: CaMKII ratio = 18%) based on previous reports (Rangamani et al., 2016). To evaluate whether PP1 quantity controls the ppERK non-linear response, we repeated simulations with different quantities of PP1 (10, 50, and 100 % of CaMKII quantity). Model simulations show that both ppERK and phosphorylated CaMKII decrease as PP1 concentration increases (Figure 4D). The calcium duration producing half-maximal ppERK did not change much with increased PP1, however, the *sensitivity* to calcium duration decreased with an increase in PP1 (Figure 4E, Table 3). Thus, our data demonstrate that PP1 indirectly influences ppERK amplitude and sensitivity to calcium duration through modulation of pCaMKII. Therefore, the ultrasensitivity of both CaMKII and ppERK depends on the ratio of CaMKII to PP1 quantity.

CaMKII does not directly activate ERK but instead modulates ERK phosphorylation through its phosphorylation of SynGap, a molecule that inactivates Ras family GTPases. The effect of CaMKII phosphorylation is complex, including enhanced SynGap activity (Walkup IV et al., 2015) and SynGap dispersion from the spine (Araki et al., 2015). We evaluated the contribution of these processes by eliminating them individually. Simulations reveal that persistent activation of ERK requires phosphorylation of SynGap by pCaMKII and dispersion of pSynGap to the dendrite (Figure 4F). A lower ppERK total activity results when pSynGap remains anchored in the spine (Figure 1B, Figure 4F, no pSynGap dispersion trace). Blocking the phosphorylation of SynGap was implemented using two approaches. In one, CaMKII can bind to SynGap but does not phosphorylate it. This reduces the available SynGap, which doubles ppERK concentration compared to control (Figure 4F, pCK bound to SynGap). In the second approach, CaMKII is unable to bind to SynGap. This increases the available SynGap, resulting in a reduction of ppERK below basal (Figure 4F, no pCK bound to SynGap). These data suggest that the quantity of free SynGap in the spine, which is controlled by CaMKII, regulates ERK activation. To verify that the results were not an artifact of the binding affinity implemented in the model, simulations were repeated using 10x and 100x lower affinity of pCaMKII for SynGap. Simulation results show a similar relation of ppERK to pSynGap, reinforcing the hypothesis that CaMKII regulates ppERK total activity through its modulation of SynGap.

Overall ppERK response is a linear combination of response to calcium and cAMP

Simulations reveal that both pathways (calcium, cAMP) combine linearly to activate ERK. Figure 5A shows that the response to stimulating both pathways overlaps with the sum of the single pathway responses. This summation was observed with short and long duration stimuli and with high and low amplitude stimuli, regardless of whether calcium was below or above the

threshold. When calcium is below threshold (e.g. short duration stimuli), cAMP contributes more to ppERK, whereas when calcium is above the threshold, it provides most of the ppERK (Figure 5B). The contribution of cAMP is transient, occurring briefly after induction while the calcium contribution is delayed and sustained (Figure 5C). The two pathways have distinct temporal dynamics that overlap and switch in their contribution about 3 min after induction. Further subdividing pathway contributions (Figure 5D) reveals that the transient ppERK is produced by Epac, with PKA and Gi contributing to a small sustained ppERK. Most of the sustained ppERK is produced by SynGap, with RasGRF contributing to a small transient ppERK.

In summary, ppERK exhibits a non-linear response to calcium, a linear response to cAMP pathways, and the response to the combination of pathways also is a linear combination of the single pathway responses. Nevertheless, each pathway exhibits distinct temporal pattern dynamics. However, these simulations used single pulses of stimuli; thus, the next section evaluates the response to stimuli similar to those used for synaptic plasticity experiments.

L-LTP stimuli: ERK signaling pathway temporally integrates input signals

Previous research has shown that different temporal patterns for inducing L-LTP work through different signaling pathways: PKA is needed for spaced stimuli while CaMKII is greater in response to massed stimuli. Thus, a critical question is whether different temporal patterns select different signaling pathways for activation of ERK. To evaluate that question, we simulated the response to L-LTP inputs. As in L-LTP experiments, the model was activated with four trains of 100 Hz stimuli for 1 sec using a range of inter-train intervals (ITIs), including massed (3,20, 40 sec) and spaced (80,300 sec) ITI.

Temporal sensitivity of ppERK to cAMP matches that of PKA

Since ppERK increases more with cAMP duration than concentration (either direct action or in combination with Giβγ), as shown above, we predicted that ppERK would be greater for spaced than massed stimulation with cAMP. Model simulations with cAMP input show that ppERK total activity increases as ITI increases (Figure 6). Note that the ppERK amplitude decreases with ITI (Figure 6A), but the increase in ppERK duration more than compensates for the lower amplitude, resulting in greater total activity for the 300 sec ITI. The summation is significantly higher than the combination as observed with single-pulse stimuli: ppERK in response to Giβγ plus Epac and PKA pathways is less than the sum of the responses to either pathway alone (Figure 6B). Competition for Src and Rap1GDP, which limits linear summation, is also observed for L-LTP stimuli. Note that the temporal sensitivity of ppERK is similar to that of PKA (Figure 6B). However, the Epac pathway contributes more to ppERK with short ITI while PKA contributes more with spaced stimuli (Figure 6 - Supplementary Figure 1), suggesting an Epac dependent L-LTP for short ITIs. In summary, ERK activated by cAMP exhibits sensitivity to ITI and is greater with spaced stimuli. These data are consistent with experiments showing a requirement for PKA in spaced but not massed stimulation, and simulations showing an increase in PKA activity with spaced stimulation (Kim et al., 2010; Woo et al., 2003).

ppERK favors longer ITIs, independent of CaMKII temporal sensitivity

L-LTP simulations using 1 μM amplitude calcium pulses produce similar ppERK traces for ITIs between 3 and 40 sec (Figure 7A). Multiple 1 sec pulses of 1 μM calcium are similar to a single 5 sec pulse, due to the slow decay of pCaMKII; thus, calcium is above the threshold for CaMKII ultrasensitivity and ppERK is sustained for a long duration, consistent with experimental data showing that CaMKII above threshold is enough to induce sustain L-LTP

(Shibata et al., 2021). Only with a 300 sec ITI does pCaMKII and ppERK decay (though not to basal) between stimuli. The temporal sensitivity of ppERK in response to calcium input tends toward longer ITIs than the temporal sensitivity of CaMKII. The greatest total activity of ppERK (Figure 7B) and pCaMKII (Figure 7C) are observed with 80 sec and 3 sec ITI, respectively. To test the role of CaMKII ultrasensitivity in the temporal sensitivity of ppERK, we repeated simulations with an increased PP1 quantity (10 µM, or 50% ratio). As observed with 18% PP1, the greatest pCaMKII occurs with short ITIs, as reported previously (Ajay and Bhalla, 2004; Kim et al., 2010), but the decrease in pCaMKII with ITI is steeper with 50% PP1. This change shifted ppERK temporal sensitivity slightly to favor middle ITIs but still does not match the temporal sensitivity of CaMKII.

In addition to varying PP1 quantity, we used lower concentration calcium pulses and an alternative CaMKII model (alt CaMKII) (Dupont et al., 2003; J□drzejewska-Szmek et al., 2017) that does not exhibit the same ultrasensitivity. Simulations with this alternative CaMKII model reveal a small shift in temporal sensitivity toward smaller ITIs, but the temporal sensitivity of ppERK still tends toward longer ITIs than the temporal sensitivity of CaMKII. Similar results were observed with the ultrasensitive CaMKII model when smaller calcium pulses (0.5 µM) were used (Figure 7 B&C). In addition, ERK's temporal sensitivity follows RasGRF (low calcium) and SynGap (high calcium) temporal activity (Figure 7 - Supplementary Figure 1). Similar to what was observed with single-pulse experiments, either blocking dispersion of SynGap or blocking pCaMKII binding to SynGap reduces ppERK (Figure 7 - Supplementary Figure 2). In summary, though the ultrasensitivity of CaMKII is controlled in part by PP1, ppERK temporal sensitivity does not follow CaMKII temporal sensitivity, and instead follows the temporal sensitivity of CaMKII downstream targets such as SynGap.

ppERK favors long intertrial intervals

To simulate L-LTP in response to 4 trains of synaptic activation, we used both calcium and cAMP inputs, as would occur with glutamatergic inputs. L-LTP simulations with both calcium and cAMP show an increase of ppERK total activity with longer ITI. Results show that the greatest total ppERK occurs at 80 sec (using 18 % PP1 and 1 µM calcium) or 300 sec (using 50% PP1-1 µM calcium or 18% PP1-0.5 µM calcium) (Figure 8A). Though the change in optimal ITI varies little, the total quantity of ppERK greatly depends on calcium and PP1 concentration. In these simulations, the contribution of the cAMP pathway to ppERK is independent of calcium. To address the question of which pathway contributes more to ppERK and whether different temporal patterns use different pathways, we calculated the percent ppERK produced by each pathway. cAMP is responsible for a majority of the ppERK with below threshold calcium, but only responsible for a third of the ppERK for above threshold calcium (Figure 8B). Analyzing the five pathways separately reveals ppERK increases with ITI for all pathways (Figure 8 - Supplementary Figure 1). Nonetheless, the relative contribution of SynGap decreases with ITI, as the other pathways increase more with ITI (Figure 8C). As seen with single-pulse stimuli, pSynGap is the main source of prolonged ppERK, whereas Epac and RasGRF are main sources of transient ppERK (Figure 8 - Supplementary Figure 2).

ppERK linearly integrates the calcium and cAMP inputs when calcium is below threshold. Thus, the response to the combined stimuli is similar to the sum of ppERK responses to individual stimuli with 0.5 µM calcium (Figure 8A). Similar results were obtained with 50% PP1. With 18% PP1 and high calcium (above threshold), supralinear summation was observed: the response of the combination is greater than the summation of individual responses (Figure 8A). CaMKII modulation of SynGap with above threshold calcium may be responsible for the

supralinear summation as SynGap dispersion enhances RasGTP and Rap1GTP in response to cAMP.

To further investigate responses to synaptic input, we simulated our model with five different L-LTP protocols. Two of them, bath-applied isoproterenol (ISO) followed by either 1 sec of 100 Hz stimulation or 180 sec of 5 Hz, experimentally elicit LTP, whereas giving 100 Hz, 5 Hz or ISO alone do not. For these protocols, cAMP, calcium, and Gi inputs were determined from a spatial model response to glutamate (J□drzejewska-Szmek et al., 2017); thus, cAMP is produced by Gs and calcium-calmodulin activation of adenylyl cyclase. Simulation results show that isoproterenol followed by either 100 Hz or 5 Hz produce greater ppERK than ISO, 100 Hz or 5 Hz alone (Figure 9). These results are consistent with experimental observations (Gelinas et al., 2008a, 2008b; Winder et al., 1999) that the combination stimuli are needed to produce L-LTP, thus validating the model. In addition, our results show that cAMP provided by ISO is compensating for the strong calcium input provided by four trains of 100 Hz.

We performed additional simulations to evaluate the role of Ras and Raf isoforms and to further validate the model. First, we simulated Raf knockout experiments and measured ERK activity in response to 4 train of 100 Hz. Simulation results are consistent with experimental data (Chen et al., 2006; Li et al., 2016; Takahashi et al., 2017; York et al., 1998) as bRaf knockout, but not Raf1 knockout, greatly reduces ERK activity (Figure 8 - Supplementary Figure 3A). Second, we simulated Ras or Rap knockout and measured ERK activity after LTP induction. Simulation results are consistent with experimental data (Grewal et al., 2000b, 2000a; Keyes et al., 2020; Li et al., 2016; Takahashi et al., 2013; York et al., 1998; Zhang et al., 2018) as knocking out Rap1 produces a greater ppERK deficit than knocking out Ras (Figure 8 - Supplementary Figure 3B). We assessed whether Ras could compensate for Rap and vice versa,

by doubling the quantity of the remaining GTPase. Result shows that doubling Ras cannot compensate for the Rap1 knockout, whereas doubling Rap1 increases ppERK above the control (Figure 8 - Supplementary Figure 3B2). This shows, for the first time, that overexpression of Rap1 can compensate for Ras activity in ERK activation.

A unique aspect of our model is that full activation of Raf1-RasGTP requires dimerization; thus, we evaluated the impact of dimerization on ERK activation. Dimerization reduces the temporal sensitivity of ppERK (Figure 8 - Supplementary Figure 3A), as the difference in ppERK between 3 sec and 300 sec ITIs is much larger when dimerization does not occur. The biggest effect is a reduction in ppERK at short ITIs; thus, dimerization enhances ppERK mostly for short ITIs.

In summary, these results demonstrate that ERK signaling pathways integrate multiple inputs synergistically. In fact, ppERK activity in response to the combination of calcium and cAMP is always greater than the response to either calcium or cAMP alone. For high calcium inputs, as likely occur during L-LTP induction, these inputs combine supralinearly. Synergy is attributable to CaMKII phosphorylation of SynGap, as dispersion of SynGap from the spine enhances RasGTP and RapGTP in response to both calcium and cAMP inputs. Furthermore, our simulations suggest that Raf dimerization enhances Raf1 activation of ERK in response short ITI, thereby reducing the temporal sensitivity of ERK activation.

Robustness

In computational models, it is critical to ensure the robustness of the results to variation in parameter values. The main result of the model is that ERK signaling pathways, no matter the protocol used, favor spaced stimuli. To assess the robustness of the temporal sensitivity of ERK

signaling pathway to small variations in parameters, simulations were repeated using concentrations of ±10% of the control value. The concentrations were changed either individually or collectively with changes drawn from a uniform distribution (between -10% and +10%). These simulations show that total ERK increase with ITI, similar to control results. Table 4 shows that the optimal ITI was 80 or 300 sec (spaced) 80% of the time. We also evaluated the mean ppERK (across all ITIs) and the degree of temporal sensitivity, quantified as the difference between maximum ppERK and minimum ppERK (across ITIs). Results show that a 10% change in a single molecule quantity rarely produced more than 20% change in mean ppERK (Figure 10A), with changes evenly distributed about 0%. In contrast, temporal sensitivity was more sensitive to parameter variations, with most parameter changes increasing temporal sensitivity (Figure 10B). An increase in temporal sensitivity with minimal change in mean ppERK implies that the response to short ITIs decrease while the response to long ITIs increase. As observed with single molecule changes, small random changes to all molecule quantities increased temporal sensitivity (Figure 10B) with minimal changes in mean ppERK (Figure 10A).

To evaluate which molecule quantities produced the largest effect on ppERK, we used random forest regression to analyze the effect of random changes on the entire set of molecules. Random forest regression is a non-linear method (in contrast to linear regression) to determine which parameters are best for predicting the results. The algorithm creates numerous decision trees, each of which is a hierarchical set of rules, where each rule partitions the data (ppERK in our case) based on a single feature (molecule quantity in our case). The features of each tree are ranked based on their weight in accurately predicting the data. Table 5 ranks the molecules, with the highest weight indicating the molecule that caused the most significant change in ppERK. The observation that most weights are small indicates that no single molecules can explain the

change in ppERK. However, calcium pathway molecules such as RasGRF, calmodulin, pmca, and cAMP pathway such as Epac are ranked high, consistent with the contribution illustrated in single pathway simulations. In summary, the temporal sensitivity of ERK is quite robust to variation in parameters and favors spaced ITIs.

Discussion

Numerous experiments have demonstrated that ERK is critical in L-LTP induction: ERK phosphorylates transcription factors, molecules involved in protein translation, and regulates cell excitability through ion channel phosphorylation. ERK is activated through numerous pathways; however, it is unclear why so many pathways converge on ERK. Furthermore, some pathways are required, whereas other pathways can be compensated. Due to complicated interactions, models of signaling pathways are crucial for understanding the molecular foundations of L-LTP. Using a computational model of signaling pathways underlying L-LTP in hippocampus CA1, we evaluated temporal sensitivity and synergy between the ERK pathways utilized by different L-LTP stimulation protocols. Our data demonstrate that calcium and cAMP work synergistically to activate ERK, and we show for the first time the role of SynGAP in mediating the synergy between pathways. SynGAP mutations are associated with a variety of syndromes, such as autism and intellectual disability. Our simulations suggest that this phenotype might be in part caused by dynamics of ERK activation following closely the dynamics of SynGAP dispersion from the spine. Our data also show that stimuli spaced in time activate more ERK than stimuli massed in time, a temporal sensitivity similar to PKA but different than CaMKII. These ERK activation pathways are not redundant as each has a distinct dynamic, contributing to different time frames of ERK activation. For example, Epac contributes to an early transient ERK activation, whereas PKA contributes to a later transient ERK activation. With massed stimuli,

calcium produces a rapid and sustained ERK activation, whereas with spaced stimuli, calcium only produces small transient ERK responses. The difference in dynamics and contribution of each pathway reinforce how neurons are able to recognize and discriminate different patterns in learning protocols.

The model elucidates that CaMKII contributes to ERK activation through phosphorylation of SynGap. This synaptic RasGap, selectively expressed in the brain, regulates ERK activity by inactivating RasGTP and Rap1GTP (Gamache et al., 2020; Pena et al., 2008). CaMKII phosphorylation of SynGap both increases its activity (Walkup IV et al., 2015) and causes dispersion to the dendrite (Araki et al., 2015). To investigate the role of dispersion, we repeated simulations without dispersion of pSynGap and observed that the ppERK amplitude was decreased by half. This effect is observed because its activity is doubled in the spine, reducing the available quantity of RasGTP and Rap1GTP. Thus, the dispersion of pSynGap attenuates its activity in the spine, which allows a long-lasting spine enlargement as observed in experiments (Araki et al., 2015). We also showed that blocking CaMKII binding to SynGap greatly reduced ppERK activity, whereas allowing CaMKII to bind but not phosphorylate SynGap greatly increased ppERK activity. This result is consistent with experiments (Rumbaugh et al., 2006) showing that overexpression or depletion of SynGap significantly reduced and enhance ERK activity, respectively. Thus, CaMKII-dependent pathway SynGAP dispersion from the synaptic spine activity controls ERK recruitment.

One of our main conclusions is that feedforward loops can support ERK activation for L-LTP induction without PKC. Induction refers to the transient events that trigger the formation of L-LTP while maintenance refers to the persistence of biochemical signaling that supports L-LTP. Our results showed that ppERK decays in less than an hour, suggesting that ERK is required

during induction of L-LTP but not during maintenance, which lasts for multiple hours. These results are consistent with experiments showing that inhibition of ERK 30 minutes after induction does not block LTP (Kelleher et al., 2004). PKMζ, the atypical form of PKC, participates in a feedforward loop to support L-LTP maintenance (Ajay and Bhalla, 2004; Tsokas et al., 2016); however, the evidence that PKC is required for L-LTP induction is weak, and thus we did not include it in our model. Similarly, we did not include metabotropic glutamate receptors, which activate PKC, because structural plasticity, a correlate of LTP, is independent of mGluR stimulation (Zhai et al., 2013). An alternative feedforward loop involves PKA inhibiting ERK inactivation mechanisms (Neves et al. 2008), but PKA is not required for all forms of L-LTP induction. Our model reveals an additional feedforward loop, connecting CaMKII to SynGap to ERK, which is activated during L-LTP induction. This pathway may be critical for induction of L-LTP in CA1 for protocols resistant to inhibition of PKA and PKC (Sweatt, 1999). In summary, our study supports prior results showing that feedforward loops are sufficient to activate ERK but reveals a novel feedforward loop involving SynGap.

Temporal selectivity is an important characteristic of learning and memory formation. Animals can learn to respond similarly to a variety of temporal patterns, or can respond differently depending on the temporal pattern (Delamater and Holland, 2008; Mauk and Ruiz, 1992). In some cases, synaptic input can produce either LTD or LTP depending on the temporal frequency of the input (Chen et al., 2010; Hawes et al., 2013). In other words, neurons can discriminate and respond differently to these different temporal input patterns (Bhalla, 2017), but also need to be able to learn despite a difference in temporal patterns. We showed that ERK is activated for a wide range of temporal input patterns, but what are the differences allowing temporal pattern discrimination?

One mechanism for temporal pattern discrimination is the temporal pattern of ERK itself, which can determine whether a cell differentiates or divides (Santos et al., 2007; Sasagawa et al., 2005; von Kriegsheim et al., 2009), and whether LTP and LTD occur (Thiels et al., 2002). We have summarized kinase activity as area under the curve, but some downstream molecules may be more sensitive to dynamics or peak activity. Indeed, our data show repeated transients of ppERK with 300 ITI versus a sustained ppERK with 80 and smaller ITIs, and the peak activity of ERK has a different temporal sensitivity than total activity. Total activity increases with ITI while peak decreases with ITI, implying that processes sensitive to peak versus AUC could distinguish these temporal patterns. We predict that these temporal patterns can be decoded by the nucleus to produce different gene expression patterns, as previously suggested (Jain and Bhalla 2014). Our model prediction of different ERK dynamics could be tested using the new EKAR sensor to image ERK activation in hippocampal slices after L-LTP induction using different ITIs, and the prediction of different gene expression patterns could be tested using some of the newer gene expression techniques, e.g.TRAP-seq (McKeever et al., 2017), to determine whether short ITIs produced different gene expression patterns than long ITIs.

A second mechanism for temporal pattern discrimination is that pathways activating ERK have other targets essential for L-LTP induction. Our results show that the CaMKII and calcium contribution to ERK decreases with ITI, whereas the PKA and cAMP contribution to ERK increases with ITI. The opposite temporal sensitivity of these critical kinases, as previously reported (Ajay and Bhalla, 2004, 2004; Kim et al., 2010; Woo et al., 2003), can contribute to pattern discrimination by the neuron, through activation of other downstream molecules that are required for LTP. For example, re-organization of the actin cytoskeleton (Borovac et al., 2018; Honkura et al., 2008; Obashi et al., 2019) is required to increase the size of the spine to allow for

more glutamate receptors. In particular, both CaMKII and PKA control actin binding proteins, such as cofilin (Havekes et al., 2016; Zhao et al., 2012). Thus, even in cases where ERK activity cannot distinguish temporal patterns, the temporal sensitivity of other key kinases can contribute to temporal pattern sensitivity.

Our results suggest that numerous signaling pathways activate ERK to enhance sensitivity to a range of temporal patterns, but there are other differences between the pathways that suggest they are not redundant. If those pathways were redundant, then, contrary to experimental observations (Gelinas et al., 2008b, 2008a; Scharf et al., 2002; Woo et al., 2003), blocking one of them should not block ERK dependent L-LTP. In addition, our model predicts that Rap1 and Ras are not interchangeable: Rap1 can compensate for Ras, but Ras cannot compensate for Rap1. Instead of redundancy, multiple pathways may be needed to control ERK dynamics and allow it to perform multiple tasks. For example, Sasagawa et al., 2005, demonstrated that there are two distinct dynamics of ERK, transient and sustained, due to the distinct timeframe of Ras and Rap. Similarly, we observed that each ERK activation pathway has a distinct dynamic, each contributing to a different time frame of ERK activation. For example, Epac contributed to an early transient ERK activation, whereas PKA contributed to a later transient ERK activation, and CaMKII produced a sustained ERK activation. Thus, our model predicts that an Epac knockout would lead to slower ERK activation. These different time frames of ERK may phosphorylate different targets (Keyes et al., 2020; Zhai et al., 2013; Zhang et al., 2018). For example, Epac, a molecule of emerging importance in neurodevelopmental disorders, may have a role in disorders in cAMP degradation by enhancing the early activation of ERK. SynGap may be critical for a pool of ERK in the spine, whereas PKA may be essential for a pool of ERK that translocates to the nucleus. In this context, we predict that overexpression of SynGap would not reduce ERK

activity in the nucleus but only in the spine. An experimental test of this prediction could use EKAR imaging (Harvey et al., 2008) to quantify ERK expression in the spine versus nucleus or measure gene expression with overexpression of SynGap.

Different temporal patterns may produce different outcomes by activating different pools of ERK. Studies have shown that scaffolding proteins, such as Kinase Suppressor of Ras (KSR) protein (Dougherty et al., 2009; Shalin et al., 2006) and β-arrestins (Bourquard et al., 2015; DeFea et al., 2000), can create multi-protein complexes of ERK, MEK and Raf, and dictate the subcellular location of ERK activity. Thus, a critical question is whether the spatial pool of ERK depends on which signaling pathways are activated during induction of LTP. These different pools of ERK may perform different functions, such as translocating to the nucleus to initiate gene transcription, staying in the cytoplasm to initiate local changes in excitability, or allowing stimulated spines to capture newly synthesized proteins to enable persistence of L-LTP (as in synaptic tagging and capture) (Frey and Morris, 1997; Redondo et al., 2010; Sajikumar et al., 2007; Young et al., 2006). This leads to a second question regarding what limits the spatial spread of molecules involved in marking spines as having been stimulated. In this context, a possible role for SynGAP dispersion would be to limit diffusion of active Ras family proteins to nearby, non-stimulated spines, thereby creating microdomains of ERK. Spatial models (Bhalla, 2017; Kim et al., 2011) have shown that buffering and other inactivation mechanisms can produce spine-sized microdomains of calcium and cAMP, but not PKA or CaMKII, suggesting additional mechanisms may be needed to produce spine-sized microdomains of ERK. Taking those questions together it will be quite interesting to implement a spatial model to investigate mechanisms that govern spatial pools of ERK and spatial and tagging specificity.

METHODS

Computational methods

To investigate how temporal pattern of synaptic activity determines which pathway in the ERK signaling cascade (Figure 1A, Figure 1- Supplementary Tables 1&2) dominates in dendritic spines of hippocampal CA1 pyramidal neurons, we developed a single compartment, stochastic reaction-diffusion model of pathways activating ERK. The model was built by merging and adapting two existing models of synaptic plasticity in hippocampal neurons. One of those models (J□drzejewska-Szmek et al., 2017) explains how different temporal patterns activate different kinases such as CaMKII and PKA that are critical for L-LTP induction, and the other model (Jain and Bhalla, 2014) demonstrates that protein synthesis is the result of synergistic activation of different pathways such as ERK and mTOR to generate unique patterns in response to different L-LTP stimuli. These previously published models were modified by adding several molecules and reactions critical for ERK activation.

One major change to the merged model is C-Raf dimerization. Dimerization regulates C-Raf activation and its subcellular localization (Desideri et al., 2015; Garnett et al., 2005). Full activation of C-Raf, but not B-Raf, requires dimerization. RasGTP binds to C-Raf to form an inactive complex, C-Raf-RasGTP, which then homodimerizes to become active, thus able to phosphorylate MEK that activates ERK. Another major change is the addition of two important molecules, RasGRF and SynGap, involved in hippocampal LTP (Araki et al., 2015; Darcy et al., 2014; Jin and Feig, 2010; Kim et al., 1998; Li et al., 2006). RasGRF is activated by binding to calcium-calmodulin; once activated, RasGRF binds to RasGDP and allows the exchange of GDP for GTP. SynGap inactivates Rap1GTP and RasGTP with low affinity. Once phosphorylated by

CaMKII, SynGAP affinity doubles towards RasGTP and Rap1GTP and causes SynGAP dispersion from synapses to the dendrite.

Initial conditions and rate constants are either taken from previous models (Jain and Bhalla, 2014; J□drzejewska-Szmek et al., 2017) or adjusted to reproduce experimentally measured concentrations of molecules (Figure 1 - Supplementary Table1&2) or to match time course data, e.g. rate constants governing CaMKII autophosphorylation. The concentration of some species was adjusted to produce an intracellular concentration of calcium of ~50 nM and cAMP of ~30 nM, among others. For example, the concentration of PDEs was adjusted to produce a 30 nM basal of cAMP. Calcium extrusion mechanisms and the low affinity and immobile calcium buffer were adjusted to obtain a steady-state of about 50 nM of internal calcium. To match the *in vitro* data on basal concentration, we ran the model for about an hour to obtain steady-state concentrations for all molecules.

Several simulations use a compartment with a volume comparable to a spine head (about 0.1 to 0.8 μm^3). To minimize noise inherent in stochastic models, most simulations used a larger compartment, of volume 4 μm^3. Other than the level of noise, no differences in temporal sensitivity were observed between the small and large volume models.

Stimulation protocols

In brain slices, presynaptic stimulation results in calcium influx through NMDA receptors, and norepinephrine (NE) or dopamine, which bind to Gs-coupled metabotropic receptors (J□drzejewska-Szmek et al., 2017) is required for L-LTP (Huang and Kandel, 1995). To investigate the effect of calcium distinct from cAMP produced by NE, the model is activated using three independent inputs leading to ERK activation: calcium (through RasGRF and

SynGap), cAMP (through Epac and PKA), and βγ subunit of inhibitory G protein (Gi) (through implicit PKA phosphorylation of βAR). βARs are mostly coupled with stimulatory G protein (Gs). However, when phosphorylated by PKA, βARs decouple from Gs and couple with inhibitory G proteins (Gi). Both Gs-activated and βAR coupled to Gi-activated signaling pathways converge to activate ERK using different pathways. To determine if maximal ERK activation requires multiple pathways, the contribution of each pathway was tested singly and in combination using either a duration or amplitude protocol (Table 1). Duration protocols used a sustained concentration of calcium, cAMP, and Giβγ. Amplitude protocols used transient (1 sec duration) elevations of different concentrations of the inputs. Calcium and cAMP each have several different pathways to ERK activation; thus, to determine the contribution of each of the (sub)pathways, the above simulations were repeated with one of the rates set to zero, as shown in Table 2. To investigate whether different L-LTP temporal patterns select different signaling pathways for ERK activation, simulations were performed using stimulation protocols identical to the experimental protocols used to induce L-LTP. Therefore, we stimulated the model with four trains of 100 Hz for 1 sec at five different intertrial intervals: 3, 20, 40sec (massed) or 80 and 300 sec (spaced) (Figure 1C). Each stimulation pulse triggered a transient release of either calcium, cAMP (direct action, and in combination with Giβγ) singly or in combination.

We also tested different forms of stimulation patterns that induce L-LTP. The additional stimulation protocols are bath applied isoproterenol (ISO) followed by 1 train of 100 Hz (ISO+100Hz) or 5 Hz (ISO+5 Hz). The inputs used to run these simulations are derived from simulations of a spatial model response to glutamate (J□drzejewska-Szmek et al., 2017).

Simulation and Analysis

The model is implemented using a stochastic reaction-diffusion simulator NeuroRD (J□drzejewski-Szmek and Blackwell, 2016), version 3.2.4 (https://github.com/neurord/stochdiff/releases), using the adaptive (asynchronous tau-leap) numerical method and tolerance of 0.1. All model files needed to run the simulations, including molecule quantities, reaction rate constants, and stimulation quantities are available on GitHub (https://github.com/neurord/ERK).

Biochemical experiments assess kinase activity by measuring the change in concentration of the product after a specific time. Thus, in these simulations, the kinase activity is quantified as total activity over simulated time compared to the activity under conditions of no stimulation, also known as Area Under the Curve (AUC). To account for stochastic variation, simulations were repeated five times (each using a different random seed) and results presented are the mean and standard error over the trials. The sample size is based on previous publications (J□drzejewski-Szmek and Blackwell, 2016), which found this sample size sufficient to show differences between conditions. Analysis was done in Python 3, using nrdh5_analV2.py available on GitHub (https://github.com/neurord/NeuroRDanal).

Statistical analysis was done in Python3 (https://github.com/neurord/ERK/tree/master/Analysis). To whether the response was linear, the AUC versus stimulation duration or concentration was fit to a line, a Hill equation, and a logarithmic equation (the latter two selected subjectively as matching the shape of the curve). The response was considered non-linear if both adjusted R^2 and Akaike Information Criteria (AIC) were better for one of the non-linear equations. To determine whether two pathways combined linearly, analysis of variance was used, with AUC of doubly phosphorylated ERK

(ppERK) as the dependent variable, and intertrial interval and stimulation type (combination or summation) as independent variables (N=5 in each group). Random forest regression was used to analyze the robustness simulations, to determine which parameter values had the most influence on the change in ppERK AUC. Random forest, a non-linear method of regression that creates multiple decision trees. Each tree is made by randomly selecting features, e.g. molecule concentration, that best predict the dependent variable, i.e. ppERK. By using a large number of decision trees (100 for this analysis), the results are quite robust. The outcome of the random forest is a weight for each feature, indicating its usefulness in predicting the dependent variable. By design, the sum of weights for all features equals 1.

REFERENCES

1. Ajay, S.M., Bhalla, U.S., 2007. A propagating ERKII switch forms zones of elevated dendritic activation correlated with plasticity. HFSP J 1, 49–66.
2. Ajay, S.M., Bhalla, U.S., 2004. A role for ERKII in synaptic pattern selectivity on the time-scale of minutes. European Journal of Neuroscience 20, 2671–2680.
3. Araki, Y., Zeng, M., Zhang, M., Huganir, R.L., 2015. Rapid Dispersion of SynGAP from Synaptic Spines Triggers AMPA Receptor Insertion and Spine Enlargement during LTP. Neuron 85, 173–189.
4. Bhalla, U.S., 2017. Synaptic input sequence discrimination on behavioral timescales mediated by reaction-diffusion chemistry in dendrites. eLife 6, e25827.
5. Borovac, J., Bosch, M., Okamoto, K., 2018. Regulation of actin dynamics during structural plasticity of dendritic spines: Signaling messengers and actin-binding proteins. Molecular and Cellular Neuroscience, Membrane Trafficking and Cytoskeletal Dynamics in Neuronal Function 91, 122–130.
6. Bourquard, T., Landomiel, F., Reiter, E., Crépieux, P., Ritchie, D.W., Azé, J., Poupon, A., 2015. Unraveling the molecular architecture of a G protein-coupled receptor/β-arrestin/Erk module complex. Scientific Reports 5, 10760.
7. Bradshaw, J.M., Kubota, Y., Meyer, T., Schulman, H., 2003. An ultrasensitive Ca2+/calmodulin-dependent protein kinase II-protein phosphatase 1 switch facilitates specificity in postsynaptic calcium signaling. Proc Natl Acad Sci USA 100, 10512–10517.
8. Buscà, R., Pouysségur, J., Lenormand, P., 2016. ERK1 and ERK2 Map Kinases: Specific Roles or Functional Redundancy? Frontiers in Cell and Developmental Biology 4,53.
9. Çalışkan, G., Stork, O., 2018. Hippocampal network oscillations as mediators of behavioural metaplasticity: Insights from emotional learning. Neurobiology of Learning and Memory, Behavioral Metaplasticity 154, 37–53.
10. Chen, A.P., Ohno, M., Giese, K.P., Kühn, R., Chen, R.L., Silva, A.J., 2006. Forebrain-specific knockout of B-raf kinase leads to deficits in hippocampal long-term potentiation, learning, and memory. Journal of Neuroscience Research 83, 28–38.
11. Chen, Ling, Cai, W., Chen, Lei, Zhou, R., Furuya, K., Sokabe, M., 2010. Modulatory metaplasticity induced by pregnenolone sulfate in the rat hippocampus: A leftward shift in LTP/LTD-frequency curve. Hippocampus 20, 499–512.
12. Darcy, M.J., Trouche, S., Jin, S.-X., Feig, L.A., 2014. Ras-GRF2 Mediates LTP, Survival and Response to an Enriched Environment of Newborn Neurons in the Hippocampus. Hippocampus 24, 1317–1329.

13. Davis, S., Vanhoutte, P., Pagès, C., Caboche, J., Laroche, S., 2000. The MAPK/ERK Cascade Targets Both Elk-1 and cAMP Response Element-Binding Protein to Control Long-Term Potentiation-Dependent Gene Expression in the Dentate Gyrus *In Vivo*. J. Neurosci. 20, 4563–4572.

14. de Rooij, J., Rehmann, H., van Triest, M., Cool, R.H., Wittinghofer, A., Bos, J.L., 2000. Mechanism of Regulation of the Epac Family of cAMP-dependent RapGEFs. J. Biol. Chem. 275, 20829–20836.

15. DeFea, K.A., Zalevsky, J., Thoma, M.S., Déry, O., Mullins, R.D., Bunnett, N.W., 2000. β-Arrestin–Dependent Endocytosis of Proteinase-Activated Receptor 2 Is Required for Intracellular Targeting of Activated Erk1/2. J Cell Biol 148, 1267–1282.

16. Delamater, A.R., Holland, P.C., 2008. The influence of CS-US interval on several different indices of learning in appetitive conditioning. J Exp Psychol Anim Behav Process 34, 202–222.

17. Desideri, E., Cavallo, A.L., Baccarini, M., 2015. Alike but Different: RAF Paralogs and Their Signaling Outputs. Cell 161, 967–970.

18. Dougherty, M.K., Ritt, D.A., Zhou, M., Specht, S.I., Monson, D.M., Veenstra, T.D., Morrison, D.K., 2009. KSR2 is a calcineurin substrate that promotes ERK cascade activation in response to calcium signals. Mol. Cell 34, 652–662.

19. Dupont, G., Houart, G., De Koninck, P., 2003. Sensitivity of CaM kinase II to the frequency of Ca2+ oscillations: a simple model. Cell Calcium 34, 485–497.

20. English, J.D., Sweatt, J.D., 1997. A Requirement for the Mitogen-activated Protein Kinase Cascade in Hippocampal Long-Term Potentiation. J. Biol. Chem. 272, 19103–19106.

21. Enserink, J.M., Christensen, A.E., de Rooij, J., van Triest, M., Schwede, F., Genieser, H.G., Døskeland, S.O., Blank, J.L., Bos, J.L., 2002. A novel Epac-specific cAMP analogue demonstrates independent regulation of Rap1 and ERK. Nature Cell Biology 4, 901–906.

22. Feig, L.A., 2011. Regulation of Neuronal Function by Ras-GRF Exchange Factors. Genes & Cancer 2, 306–319.

23. Frey, U., Morris, R.G.M., 1997. Synaptic tagging and long-term potentiation. Nature 385, 533–536.

24. Gamache, T.R., Araki, Y., Huganir, R.L., 2020. Twenty Years of SynGAP Research: From Synapses to Cognition. J. Neurosci. 40, 1596–1605.

25. Garnett, M.J., Rana, S., Paterson, H., Barford, D., Marais, R., 2005. Wild-Type and Mutant B-RAF Activate C-RAF through Distinct Mechanisms Involving Heterodimerization. Molecular Cell 20, 963–969.

26. Gelinas, J.N., Banko, J.L., Peters, M.M., Klann, E., Weeber, E.J., Nguyen, P.V., 2008a. Activation of exchange protein activated by cyclic-AMP enhances long-lasting synaptic potentiation in the hippocampus. Learning & Memory 15, 403–411.

27. Gelinas, J.N., Tenorio, G., Lemon, N., Abel, T., Nguyen, P.V., 2008b. β-Adrenergic receptor activation during distinct patterns of stimulation critically modulates the PKA-dependence of LTP in the mouse hippocampus. Learn. Mem. 15, 281–289.

28. Grewal, S.S., Fass, D.M., Yao, H., Ellig, C.L., Goodman, R.H., Stork, P.J., 2000a. Calcium and cAMP signals differentially regulate cAMP-responsive element-binding protein function via a Rap1-extracellular signal-regulated kinase pathway. J. Biol. Chem. 275, 34433–34441.

29. Grewal, S.S., Horgan, A.M., York, R.D., Withers, G.S., Banker, G.A., Stork, P.J.S., 2000b. Neuronal Calcium Activates a Rap1 and B-Raf Signaling Pathway via the Cyclic Adenosine Monophosphate-dependent Protein Kinase. J. Biol. Chem. 275, 3722–3728.

30. Harvey, C.D., Ehrhardt, A.G., Cellurale, C., Zhong, H., Yasuda, R., Davis, R.J., Svoboda, K., 2008. A genetically encoded fluorescent sensor of ERK activity. Proc Natl Acad Sci U S A 105, 19264–19269.

31. Havekes, R., Park, A.J., Tudor, J.C., Luczak, V.G., Hansen, R.T., Ferri, S.L., Bruinenberg, V.M., Poplawski, S.G., Day, J.P., Aton, S.J., Radwańska, K., Meerlo, P., Houslay, M.D., Baillie, G.S., Abel, T., 2016. Sleep deprivation causes memory deficits by negatively impacting neuronal connectivity in hippocampal area CA1. eLife 5,e13424.

32. Hawes, S.L., Gillani, F., Evans, R.C., Benkert, E.A., Blackwell, K.T., 2013. Sensitivity to theta-burst timing permits LTP in dorsal striatal adult brain slice. J Neurophysiol 110, 2027–2036.

33. Honkura, N., Matsuzaki, M., Noguchi, J., Ellis-Davies, G.C.R., Kasai, H., 2008. The Subspine Organization of Actin Fibers Regulates the Structure and Plasticity of Dendritic Spines. Neuron 57, 719–729.

34. Huang, Y.Y., Kandel, E.R., 1995. D1/D5 receptor agonists induce a protein synthesis-dependent late potentiation in the CA1 region of the hippocampus. Proc Natl Acad Sci U S A 92, 2446–2450.

35. Jain, P., Bhalla, U.S., 2014. Transcription Control Pathways Decode Patterned Synaptic Inputs into Diverse mRNA Expression Profiles. PLoS ONE 9, e95154.

36. J□drzejewska-Szmek, J., Luczak, V., Abel, T., Blackwell, K.T., 2017. β-adrenergic signaling broadly contributes to LTP induction. PLOS Computational Biology 13, e1005657.

37. J□drzejewski-Szmek, Z., Blackwell, K.T., 2016. Asynchronous τ-leaping. The Journal of Chemical Physics 144, 125104.

38. Jin, S., Feig, L.A., 2010. Long-Term Potentiation in the CA1 Hippocampus Induced by NR2A subunit-containing NMDA Glutamate Receptors Is Mediated by Ras-GRF2/Erk Map Kinase Signaling. PLoS One 5(7),e11732.

39. Kasahara, J., Fukunaga, K., Miyamoto, E., 2001. Activation of Calcium/Calmodulin-dependent Protein Kinase IV in Long Term Potentiation in the Rat Hippocampal CA1 Region*. Journal of Biological Chemistry 276, 24044–24050.

40. Kelleher, R.J., Govindarajan, A., Jung, H.-Y., Kang, H., Tonegawa, S., 2004. Translational control by MAPK signaling in long-term synaptic plasticity and memory. Cell 116, 467–479.

41. Keyes, J., Ganesan, A., Molinar-Inglis, O., Hamidzadeh, A., Zhang, Jinfan, Ling, M., Trejo, J., Levchenko, A., Zhang, Jin, 2020. Signaling diversity enabled by Rap1-regulated plasma membrane ERK with distinct temporal dynamics. Elife 9,e57410.

42. Khalilimeybodi, A., Daneshmehr, A., Sharif-Kashani, B., 2018. Investigating β-adrenergic-induced cardiac hypertrophy through computational approach: classical and non-classical pathways. J Physiol Sci 68, 503–520.

43. Kim, J.H., Liao, D., Lau, L.-F., Huganir, R.L., 1998. SynGAP: a Synaptic RasGAP that Associates with the PSD-95/SAP90 Protein Family. Neuron 20, 683–691.

44. Kim, M., Huang, T., Abel, T., Blackwell, K.T., 2010. Temporal Sensitivity of Protein Kinase A Activation in Late-Phase Long Term Potentiation. PLoS Computational Biology 6, e1000691.

45. Kim, M., Park, A.J., Havekes, R., Chay, A., Guercio, L.A., Oliveira, R.F., Abel, T., Blackwell, K.T., 2011. Colocalization of Protein Kinase A with Adenylyl Cyclase Enhances Protein Kinase A Activity during Induction of Long-Lasting Long-Term-Potentiation. PLOS Computational Biology 7, e1002084

46. Koch, W.J., Hawes, B.E., Allen, L.F., Lefkowitz, R.J., 1994. Direct evidence that Gi-coupled receptor stimulation of mitogen-activated protein kinase is mediated by G beta gamma activation of p21ras. Cell Biology 91, 12706–12710.

47. Li, S., Tian, X., Hartley, D.M., Feig, L.A., 2006. Distinct Roles for Ras-Guanine Nucleotide-Releasing Factor 1 (Ras-GRF1) and Ras-GRF2 in the Induction of Long-Term Potentiation and Long-Term Depression. J Neurosci 26, 1721–1729.

48. Li, Y., Dillon, T.J., Takahashi, M., Earley, K.T., Stork, P.J.S., 2016. Protein Kinase A-independent Ras Protein Activation Cooperates with Rap1 Protein to Mediate Activation of the Extracellular Signal-regulated Kinases (ERK) by cAMP. Journal of Biological Chemistry 291, 21584–21595.

49. Lin, C.-H., Yu, M.-C., Chiang, C.-C., Bien, M.-Y., Chien, M.-H., Chen, B.-C., 2013. Thrombin-induced NF-κB activation and IL-8/CXCL8 release is mediated by c-Src-

dependent Shc, Raf-1, and ERK pathways in lung epithelial cells. Cellular Signalling 25, 1166–1175.

50. Luttrell, L.M., Della Rocca, G.J., van Biesen, T., Luttrell, D.K., Lefkowitz, R.J., 1997. Gβγ subunits mediate Src-dependent phosphorylation of the epidermal growth factor receptor. A scaffold for G protein-coupled receptor-mediated Ras activation. J. Biol. Chem. 272, 4637–4644.

51. Malenka, R.C., Bear, M.F., 2004. LTP and LTD: An Embarrassment of Riches. Neuron 44, 5–21.

52. Mauk, M.D., Ruiz, B.P., 1992. Learning-dependent timing of Pavlovian eyelid responses: differential conditioning using multiple interstimulus intervals. Behav Neurosci 106, 666–681.

53. McKeever, P.M., Kim, T., Hesketh, A.R., MacNair, L., Miletic, D., Favrin, G., Oliver, S.G., Zhang, Z., St George-Hyslop, P., Robertson, J., 2017. Cholinergic neuron gene expression differences captured by translational profiling in a mouse model of Alzheimer's disease. Neurobiol Aging 57, 104–119.

54. Miningou, N., Blackwell, K.T., 2020. The road to ERK activation: Do neurons take alternate routes? Cellular Signalling 68, 109541.

55. Neves, S.R., Tsokas, P., Sarkar, A., Grace, E.A., Rangamani, P., Taubenfeld, S.M., Alberini, C.M., Schaff, J.C., Blitzer, R.D., Moraru, I.I., Iyengar, R., 2008. Cell Shape and Negative Links in Regulatory Motifs Together Control Spatial Information Flow in Signaling Networks. Cell 133, 666–680.

56. Obashi, K., Matsuda, A., Inoue, Y., Okabe, S., 2019. Precise Temporal Regulation of Molecular Diffusion within Dendritic Spines by Actin Polymers during Structural Plasticity. Cell Rep 27, 1503-1515.e8.

57. Pena, V., Hothorn, M., Eberth, A., Kaschau, N., Parret, A., Gremer, L., Bonneau, F., Ahmadian, M.R., Scheffzek, K., 2008. The C2 domain of SynGAP is essential for stimulation of the Rap GTPase reaction. EMBO Rep 9, 350–355.

58. Peng, S., Zhang, Y., Zhang, J., Wang, H., Ren, B., 2010. ERK in Learning and Memory: A Review of Recent Research. Int J Mol Sci 11, 222–232.

59. Rangamani, P., Levy, M.G., Khan, S., Oster, G., 2016. Paradoxical signaling regulates structural plasticity in dendritic spines. PNAS 113, E5298–E5307.

60. Redondo, R.L., Okuno, H., Spooner, P.A., Frenguelli, B.G., Bito, H., Morris, R.G.M., 2010. Synaptic tagging and capture: differential role of distinct calcium/calmodulin kinases in protein synthesis-dependent long-term potentiation. J. Neurosci. 30, 4981–4989.

61. Rumbaugh, G., Adams, J.P., Kim, J.H., Huganir, R.L., 2006. SynGAP regulates synaptic strength and mitogen-activated protein kinases in cultured neurons. Proceedings of the National Academy of Sciences 103, 4344–4351.

62. Sadowski, J.H.L.P., Jones, M.W., Mellor, J.R., 2016. Sharp-Wave Ripples Orchestrate the Induction of Synaptic Plasticity during Reactivation of Place Cell Firing Patterns in the Hippocampus. Cell Rep 14, 1916–1929.

63. Sajikumar, S., Navakkode, S., Frey, J.U., 2007. Identification of compartment- and process-specific molecules required for “synaptic tagging” during long-term potentiation and long-term depression in hippocampal CA1. J. Neurosci. 27, 5068–5080.

64. Santos, S.D.M., Verveer, P.J., Bastiaens, P.I.H., 2007. Growth factor-induced MAPK network topology shapes Erk response determining PC-12 cell fate. Nat Cell Biol 9, 324–330.

65. Sasagawa, S., Ozaki, Y., Fujita, K., Kuroda, S., 2005. Prediction and validation of the distinct dynamics of transient and sustained ERK activation. Nature Cell Biology 7, 365–373. https://doi.org/10.1038/ncb1233

66. Scharf, M.T., Woo, N.H., Lattal, K.M., Young, J.Z., Nguyen, P.V., Abel, T., 2002. Protein Synthesis Is Required for the Enhancement of Long-Term Potentiation and Long-Term Memory by Spaced Training. Journal of Neurophysiology 87, 2770–2777.

67. Schmitt, J.M., Stork, P.J.S., 2002. Gα and Gβγ Require Distinct Src-dependent Pathways to Activate Rap1 and Ras. Journal of Biological Chemistry 277, 43024–43032.

68. Schrader, L.A., Birnbaum, S.G., Nadin, B.M., Ren, Y., Bui, D., Anderson, A.E., Sweatt, J.D., 2006. ERK/MAPK regulates the Kv4.2 potassium channel by direct phosphorylation of the pore-forming subunit. American Journal of Physiology-Cell Physiology 290, C852–C861.

69. Schwechter, B., Rosenmund, C., Tolias, K.F., 2013. RasGRF2 Rac-GEF activity couples NMDA receptor calcium flux to enhanced synaptic transmission. Proceedings of the National Academy of Sciences 110, 14462–14467.

70. Shalin, S.C., Hernandez, C.M., Dougherty, M.K., Morrison, D.K., Sweatt, J.D., 2006. Kinase Suppressor of Ras1 Compartmentalizes Hippocampal Signal Transduction and Subserves Synaptic Plasticity and Memory Formation. Neuron 50, 765–779.

71. Shibata, A.C.E., Ueda, H.H., Eto, K., Onda, M., Sato, A., Ohba, T., Nabekura, J., Murakoshi, H., 2021. Photoactivatable CaMKII induces synaptic plasticity in single synapses. Nature Communications 12, 751.

72. Singh, D., Bhalla, U.S., 2018. Subunit exchange enhances information retention by CaMKII in dendritic spines. Elife 7, 22.

73. Sweatt, J.D., 2004. Mitogen-activated protein kinases in synaptic plasticity and memory. Current Opinion in Neurobiology 14, 311–317.

74. Sweatt, J.D., 1999. Toward a Molecular Explanation for Long-Term Potentiation. Learn. Mem. 6, 399–416.

75. Takahashi, M., Dillon, T.J., Liu, C., Kariya, Y., Wang, Z., Stork, P.J.S., 2013. Protein Kinase A-dependent Phosphorylation of Rap1 Regulates Its Membrane Localization and Cell Migration. Journal of Biological Chemistry 288, 27712–27723.

76. Takahashi, M., Li, Y., Dillon, T.J., Stork, P.J.S., 2017. Phosphorylation of Rap1 by cAMP-dependent Protein Kinase (PKA) Creates a Binding Site for KSR to Sustain ERK Activation by cAMP. Journal of Biological Chemistry 292, 1449–1461.

77. Tang, S., Yasuda, R., 2017. Imaging ERK and PKA Activation in Single Dendritic Spines during Structural Plasticity. Neuron 93, 1315-1324.e3.

78. Terrell, E.M., Morrison, D.K., 2019. Ras-Mediated Activation of the Raf Family Kinases. Cold Spring Harbor Perspectives in Medicine 9,a033746.

79. Thiels, E., Kanterewicz, B.I., Norman, E.D., Trzaskos, J.M., Klann, E., 2002. Long-Term Depression in the Adult Hippocampus In Vivo Involves Activation of Extracellular Signal-Regulated Kinase and Phosphorylation of Elk-1. J. Neurosci. 22, 2054–2062.

80. Tsokas, P., Hsieh, C., Yao, Y., Lesburguères, E., Wallace, E.J.C., Tcherepanov, A., Jothianandan, D., Hartley, B.R., Pan, L., Rivard, B., Farese, R.V., Sajan, M.P., Bergold, P.J., Hernández, A.I., Cottrell, J.E., Shouval, H.Z., Fenton, A.A., Sacktor, T.C., 2016. Compensation for PKMζ in long-term potentiation and spatial long-term memory in mutant mice. eLife 5, e14846.

81. von Kriegsheim, A., Baiocchi, D., Birtwistle, M., Sumpton, D., Bienvenut, W., Morrice, N., Yamada, K., Lamond, A., Kalna, G., Orton, R., Gilbert, D., Kolch, W., 2009. Cell fate decisions are specified by the dynamic ERK interactome. Nature Cell Biology 11, 1458–1464.

82. Walkup IV, W.G., Washburn, L., Sweredoski, M.J., Carlisle, H.J., Graham, R.L., Hess, S., Kennedy, M.B., 2015. Phosphorylation of Synaptic GTPase-activating Protein (synGAP) by Ca^{2+} /Calmodulin-dependent Protein Kinase II (CaMKII) and Cyclin-dependent Kinase 5 (CDK5) Alters the Ratio of Its GAP Activity toward Ras and Rap GTPases. Journal of Biological Chemistry 290, 4908–4927.

83. Wang, M., Foster, D.J., Pfeiffer, B.E., 2020. Alternating sequences of future and past behavior encoded within hippocampal theta oscillations. Science 370, 247–250.

84. Winder, D.G., Martin, K.C., Muzzio, I.A., Rohrer, D., Chruscinski, A., Kobilka, B., Kandel, E.R., 1999. ERK Plays a Regulatory Role in Induction of LTP by Theta Frequency Stimulation and Its Modulation by β-Adrenergic Receptors. Neuron 24, 715–726.

85. Woo, N.H., Duffy, S.N., Abel, T., Nguyen, P.V., 2003. Temporal spacing of synaptic stimulation critically modulates the dependence of LTP on cyclic AMP-dependent protein kinase. Hippocampus 13, 293–300.

86. York, R.D., Yao, H., Dillon, T., Ellig, C.L., Eckert, S.P., McCleskey, E.W., Stork, P.J.S., 1998. Rap1 mediates sustained MAP kinase activation induced by nerve growth factor. Nature 392, 622–626.

87. Young, J.Z., Isiegas, C., Abel, T., Nguyen, P.V., 2006. Metaplasticity of the late-phase of long-term potentiation: a critical role for protein kinase A in synaptic tagging. Eur J Neurosci 23, 1784–1794.

88. Zhai, S., Ark, E.D., Parra-Bueno, P., Yasuda, R., 2013. Long-Distance Integration of Nuclear ERK Signaling Triggered by Activation of a Few Dendritic Spines. Science 342, 1107–1111.

89. Zhang, L., Zhang, P., Wang, G., Zhang, H., Zhang, Y., Yu, Y., Zhang, M., Xiao, J., Crespo, P., Hell, J.W., Lin, L., Huganir, R.L., Zhu, J.J., 2018. Ras and Rap Signal Bidirectional Synaptic Plasticity via Distinct Subcellular Microdomains. Neuron 98, 783–800.

90. Zhao, J.-W., Gao, Z.-L., Zhang, H.-Y., Ji, Q.-Y., Wang, H., Yang, Y.-D., Xing, F., Meng, L., Wang, Y., 2012. Regulation of Cofilin Activity by CaMKII and Calcineurin. The American Journal of the Medical Sciences 344, 462–472.

MAIN FIGURES CAPTIONS

Figure 1: A. Schematic representation of signaling pathways activating ERK. Five pathways are included in the model: calcium activation of (1) RasGRF followed by RasGTP production or (2) CaMKII phosphorylation of SynGap followed by increasing RasGTP and Rap1GTP lifetime; cAMP activation of (3) Epac or (4) PKA phosphorylation of Src family kinase, leading to Rap1GTP production; Gi subtype of GTP binding protein (Giβγ) (5) recruits Src family kinase followed by activation of RasGTP. **B.** Three effects of CaMKII on SynGap were evaluated: K_{CK}. No autophosphorylation of CaMKII, K_{Syn1}. No pCaMKII binding to SynGap, K_{Syn2}. SynGap binds to pCaMKII, but cannot be phosphorylated, K_{Syn3}. SynGap phosphorylated, but not dispersed to the dendrite. **C.** LTP protocols: four trains of 100 Hz (each 1 sec duration) spaced by different intertrial intervals: 3, 20, 40, 80, and 300 sec.

The following supplements are available for figure 1:

Supplementary Table 1A: Reactions and rates constants involved in signaling pathway leading to Ras and Rap1 activation.

Supplementary Table 1B: Reaction and rates constants involved in signaling pathway of SynGap.

Supplementary Table 1C: Reactions and rates constants involved in core ERK signaling pathway

Supplementary Table 1D: Reaction and rates constants involved in signaling pathway of calcium to CaMKII.

Figure 2: Model validation: A: Time course of RasGTP in response of 30 pulses of 0.5 Hz (Harvey et al., 2008). RasGTP dynamics are qualitatively consistent with experimental measurements**. B:** Relative increase of ppERK in response to L-LTP stimuli (2 bursts of 100 Hz for 1 sec, bursts separated by 20 sec) (Kasahara et al., 2001). Simulation shows qualitative match of ERK activation to the experimental model as ppERK peaks around 3 min after stimulation and returns to basal about 30 min after stimulation.

Figure 3: Linear activation of ERK by cAMP pathways. A. ppERK response to a single pulse of 0.5 μM cAMP is graded with duration. **B.** Integral of ppERK concentration over time (AUC) in response to different cAMP concentrations (for 1 sec) and different cAMP durations (with a concentration of 0.5 μM). **C.** Time course of ppERK in response to single pulses of 0.1 μM Giβγ for different durations. Recruitment of ERK by Giβγ binding protein shows delayed activation. **D**. Total activity of ppERK in response to different Giβγ concentrations (for 1 sec) and durations (with a concentration of 0.1 μM). Increasing duration or concentration are similarly effective in increasing ppERK. **E**. Direct and indirect cAMP pathways combine linearly for all duration inputs and sub-linearly, with prolonged duration inputs. Two-way ANCOVA (analysis of covariance) of ppERK AUC versus stimulation characteristics (duration) and type (combination versus summation) as factors (N=5 in each group) is significant for both duration and type ($F(2,47) = 419.5$, $T<0.001$; $P(dur)<0.0001$, $T(dur) = 28.61$, $P(type) <0.0001$, $T(type) = 4.54$). Combo: response to Giβγ and cAMP, sum: sum of the responses in A and C. **F.** Ratio of ppERK to basal ppERK in response to cAMP activation of PKA, Epac or Giβγ (0.5 μM (Epac and PKA) or 0.1μM (Giβγ) for 30 sec). ppERK increases quickly and transiently with Epac and with a delay and more prolonged in response to PKA or Giβγ.

The following supplements are available for figure 3:

Supplementary Table 1: Regression analysis results for cAMP pathway.

Figure 4: Nonlinear activation of ERK by calcium pathway: A Time course shows a sustained ppERK when calcium is above amplitude threshold (2 μM) for 1 sec duration. **B.** Total ppERK activity over time in response to different calcium concentrations (for 1 sec) and different calcium durations (with a concentration of 0.5 μM) reveals ultrasensitive response. **C.** With CaMKII activity blocked, RasGRF is the sole calcium activated pathway to ERK activation. ERK activation is no longer ultrasensitive. **D.** pCaMKII and ppERK activities in response to 0.5 μM for 30 sec of calcium decrease with increased PP1. Similar results were observed with different concentrations or duration. **E**. Increasing PP1 quantity decreases the steepness of ppERK vs duration (log10) curve. **F.** Total ERK activity changes with SynGap availability. Blocking dispersion of SynGAP reduces ppERK, whereas allowing CaMKII to bind but not phosphorylate SynGAP enhances ppERK. **G.** Ratio of ppERK to basal ppERK in response to calcium activation of RasGRF or SynGap alone (0.5 μM calcium for 30 sec), compared with control (SynGap + RasGRF).

The following supplements are available for figure 4:

Supplementary Table 1: Regression analysis results for calcium pathway.

Figure 5: Overall ppERK response is linear combination of response to calcium and cAMP. A. Time course of ppERK response to calcium and cAMP. Calcium in combination with cAMP

traces overlaps with the sum of the single pathway responses for both short and long duration stimuli. Two-way ANCOVA (analysis of covariance) of ppERK AUC versus stimulation characteristics (duration) and type (combination versus summation) as factors (N=5 in each group) is significant for both stimulation but not type ($F(2,47) = 65.55$, $P(dur)<0.0001$, $T(stim) = 11.41$, $P(type) = 0.35$, $T(type) = -0.945$). **B.** Summary of ppERK AUC versus duration shows that the fraction of ppERK produced by calcium pathways increases with duration of the stimulation. **C.** Dynamics of ppERK, relative to basal ppERK, in response to cAMP (0.5 μM cAMP and 0.1 μM Giβγ for 30 sec), calcium (0.5 μM for 30 sec), or combination. ppERK increases transiently with cAMP and with a delay in response to calcium. Higher ppERK activation with combination (calcium and cAMP pathways). **D:** Dynamics of single pathways. Ratio of ppERK to basal ppERK in response to PKA (0.5 μM cAMP), Epac (0.5 μM cAMP), Giβγ (0.1 μM), RasGRF (0.5 μM calcium) and SynGap (pCaMKII feedforward loop; 0.5 μM calcium) for 30 sec. Epac and RasGRF produce transient ppERK whereas and PKA, Giβγ, and SynGap produce transient and sustained ppERK. C2 and D2 expand the first 100 sec after stimulation of C1 and D1, respectively.

Figure 6: ppERK favors spaced stimuli in response to cAMP input: A. Time course of ppERK in response to 4 trains of 100 Hz stimuli of cAMP (Epac, PKA, Giβγ pathways). ppERK peak amplitude decreases with ITI, but the AUC increases with ITI. **B**. Total kinase activity in response to cAMP shows that ppERK exhibits sublinear response to cAMP stimuli: the sum (dashed line) is higher than ppERK in response to combination (solid black line). PKA and ppERK have similar temporal sensitivity, favoring spaced stimuli. Two-way ANCOVA (analysis of covariance) of ppERK AUC versus stimulation characteristics (ITI) and type (combination

versus summation) as factors (N=5 in each group) is significant for both stimulation ITI and type (F (2,47) = 42.25, T<0.0001; T(ITI) = 4.67, P(ITI)<0.0001, T(type) = 7.92, P(type) <0.0001).

The following supplements are available for figure 6:

Supplementary Figure 1: Uniform ppERK temporal sensitivity within cAMP pathways.

Figure 7: ppERK favors spaced stimuli in response to calcium input, in contrast to temporal sensitivity of CaMKII. A. Time course of ppERK in response to 4 trains of 100 Hz calcium stimuli (1 μM concentration) shows sustained and prolong ppERK with 3 and 40 sec ITI. **B.** ppERK AUC changes with PP1 quantity, but still is highest for spaced ITIs. **C.** Increasing PP1 quantity or lowering calcium concentration makes CaMKII more sensitive to shorter ITIs.

The following supplements are available for figure 7:

Supplementary Figure 1: ppERK temporal sensitivity is similar to that of inactive SynGap.

Supplementary Figure 2: SynGap availability controls the magnitude of ppERK during L-LTP induction.

Figure 8: ppERK integration of calcium and cAMP inputs can be linear or supralinear. (**A**) ppERK mostly increases with temporal interval, with the greatest quantity occurring at 80 sec (above calcium threshold or 18% PP1) or 300 sec (below calcium threshold). Supralinear summation occurs at 18% PP1 and linear summation occurs at low calcium or high PP1 – conditions that reduce ultrasensitivity of CaMKII (Figure 3E). Supralinearity is indicated by the response to the combination of cAMP and calcium (Combo) is greater than the sum of responses

to calcium and cAMP separately. ANCOVA results are in Figure 8 -Supplementary table 1. **B.** Summary of ppERK total activity in response to 300 sec ITI. The contribution of the calcium pathway relative to the cAMP pathway is greatest when calcium is above threshold for an ultrasensitive CaMKII response. **C:** Qualitative single pathway contribution to ppERK (ppERK from single pathway divided by ppERK from all pathways; sum of pathways exceeds 100%). The contribution of SynGap decreases with ITI, whereas other pathways increase with ITI.

The following supplements are available for figure 8:

Supplementary Figure 1: Summary of ppERK total activity in response to each pathway.

Supplementary Figure 2: Time courses of some upstream molecules.

Figure 8- Supplementary Table 1: Results of two-way ANCOVA (analysis of covariance) of ppERK AUC versus stimulation characteristics (ITI) and type (combination versus summation).

Figure 9: ppERK predicts the occurrence of L-LTP when bath applied ISO is followed by either 1 sec of 100 Hz stimulation or 180 sec of 5 Hz. ppERK in response to isoproterenol (ISO), 1 sec of 100 Hz, or 180 sec of 5 Hz does not exceed 30 nM (A), whereas ppERK reaches or exceeds 35 nM in response to the combination of isoproterenol and either 100 Hz or 5 Hz stimulation (B).

Figure 10: ERK **Temporal sensitivity is robust to parameter variations.** Molecule concentrations were changed individually by either +10% (red) or -10% (black) or the set of concentrations was changed randomly, within ±10% (gold). **A:** Percent change in mean ppERK,

averaged across all 5 ITIs. **B:** Percent change in temporal sensitivity. Most variations increased temporal sensitivity.

SUPPLEMENTARY FIGURES AND CAPTION

Figure 6 - Supplementary Figure 1: Uniform ppERK temporal sensitivity within cAMP pathways. A: The model is stimulated using L-LTP patterns of input with only a single cAMP pathway active, either Epac, PKA, or Giβγ. Total ppERK versus ITI follows a similar pattern for all pathways, though Epac contributes more, especially for short inter-train intervals. **B:** Time courses of cAMP pathways at 3 (B1) and 300 (B2) sec ITI. Epac pathway contributes more to ppERK with 3 sec (short) ITI while PKA contributes more with 300 sec (spaced) ITI.

Figure 7 - Supplementary Figure 1: ppERK temporal sensitivity is similar to that of inactive SynGap. Normalized activity is the total activity divided by the maximum total activity (over all ITI). **Inactive SynGap** is the SynGap bound to pCaMKII or dispersed to the dendrite. **Active RasGRF** is the RasGRF bound to calmodulin. The model is simulated using L-LTP patterns of input. (**A, B**) Using 1 µM calcium, temporal sensitivity of ppERK is similar to inactive SynGap regardless of PP1 quantity. (**C**) temporal sensitivity of ppERK is similar to inactive SynGap using alternative CaMKII model, (**D**). Temporal sensitivity of ppERK matches active RasGRF more than inactive SynGap with low calcium concentration. (**E**). Pearson R was calculated between ppERK and SynGap or RasGRF. Correlation coefficients (R) demonstrate that the temporal pattern of ppERK is highly correlated with the temporal pattern of inactive SynGap, except with low calcium, in which case it is highly correlated with the temporal pattern of RasGRF.

Figure 7 - Supplementary Figure 2: SynGap availability controls the magnitude of ppERK during L-LTP induction. The model is simulated using L-LTP patterns of input with 1 µM calcium. **A**: Blocking dispersion of pSynGap to the dendrite or blocking CaMKII catalytic activity (pCaMKII bound SynGap) reduces ppERK, whereas allowing CaMKII to bind (but not phosphorylate) SynGap (No pCaMKII bound SynGap) enhances total ERK activity. **B:** Time course of ppERK produced by calcium pathways at 3 (B1) and 300 (B2) sec ITI. ERK activation by SynGap is enhanced and delayed when RasGRF is blocked.

Figure 8 - Supplementary Figure 1: Summary of ppERK total activity in response to each pathway. ppERK increases with ITI for all pathways, though SynGap does not increase as sharply, reducing its relative contribution.

Figure 8 - Supplementary Figure 2: Time courses of some upstream molecules. Time course of (A) ppERK, (B) active Epac, (C) active RasGRF, and (D) phosphorylated SynGap to four 100 Hz trains separated by 3 and 300 sec. A2-D2 represent the first 140 sec after stimulation of A1-D1, respectively.

Figure 8 - Supplementary Figure 3: A: Total ppERK activity over time in response to L-LTP stimuli under Raf1, bRaf, or Raf1 dimerization knockout (KO). bRaf is the greatest contributor, as observed experimentally. Eliminating dimerization enhances reduces ERK activation mostly for lower intertrain intervals; thus the enhanced activity of Raf1 dimers reduces temporal sensitivity of ppERK. **B:** Total ppERK activity over time in response to L-LTP stimuli under

Rap1 (C1) and Ras (C2) knockout. Rap1GTP is the main contributor to ppERK, as observed experimentally.

MAIN TABLES AND CAPTIONS

Table 1: Single pathway experiment

Input	Amplitude protocol (μM)	Duration protocol (sec)
Calcium	1 sec: 0.2, 0.3, 0.5,1,1.5,2,5	0.5 μM: 1,2,4, 5,6, 8,10,30,100 1 μM: 1,4, 100
cAMP	1 sec: 0.1,0.2,0.5,1,1.5,2	0.1 μM: 1,4,10,30,100 0.5 μM: 1,4,10,30,100
Giβγ	1 sec: 0.005,0.03, 0.1,0.5	0.03 μM: 1,4,10,30,100 0.1 μM: 1,4,10,30,100

Table 2: Knockout experiment: Rate constant names are shown in Figure 1A, B. Block lists the rate constant whose value is set to zero.

Input	Block	Effect/Molecular dependence
Calcium 2000 nM for 1 sec	K_{CK}	CaMKII is activated but cannot autophosphorylate itself, thus RasGRF is the only contributor
	K_{Syn1}	pCaMKII is unable to bind to SynGap
	K_{Syn2}	pCaMKII binds to SynGap but unable to release phosphorylated SynGap
	K_{Syn3}	SynGap is phosphorylated but unable to disperse to the dendrite
cAMP 500 nM for 30 sec	K_{Epac}	Epac binds cAMP but cannot activate Rap1GDP, thus PKA is the only contributor
	K_{PKA}	Final step of PKA pathway activation of Rap1GDP is blocked, thus Epac is the only contributor

Table 3: PP1 concentration influences ppERK quantity and ultrasensitivity. The calcium duration producing half-maximal ppERK AUC and the sensitivity to duration were estimated by fitting a hill equation to ppERK AUC vs calcium duration. Values shown are parameter estimates ± standard deviation of the estimate. Width at half max: the calcium duration at half-maximal ppERK.

PP1(%)	**Width at half max**	**Hill Coefficient**
10	6.0 ± 1.07	4.1 ± 1.5
18	6.7 ± 1.53	2.5 ± 1.1
50	9.9 ± 5.28	1.4 ± 1.1

Table 4: Count of Best ITIs: count of preferred ITIs in robustness simulations, using either single molecule changes of ± 10% or random changes (between +10% and -10%) to all molecules. 80% of the parameter variations yield optimal ppERK in response to spaced stimulation (ITI=80 or 300 sec)

ITIs	Random	10 % lower	10% higher	Total percent
3	38	0	0	4.69
20	46	0	1	5.80
40	81	3	1	10.49
80	154	112	51	39.14
300	181	40	102	39.88

Table 5: Random forest analysis: 100 random perturbations of all molecule concentrations (between +10% and -10%) were simulated. Features are ranked from most important to least important in predicting the temporal sensitivity. The sum of features' importance equals 1.

Molecules abbreviation	Weights	Molecules full name
RasGRF	0.084	Ras guanine nucleotide–releasing factor
Sos	0.074	Son of Sevenless
Cam	0.068	Calmodulin
MEK	0.050	Mitogen-activated protein Kinase Kinase
PDE2	0.050	Phosphodiesterase 2
pmca	0.048	Plasma membrane calcium pump
Epac	0.046	Exchange Protein directly Activated by cAMP
Calbin	0.046	Calbindin
CRKC3G	0.044	v-CRK Proto-Oncogene/Rap guanine nucleotide exchange factor 1
rasGap	0.043	Ras GTPase Activating Protein
SynGap	0.042	Synaptic rasGap
PP1	0.038	Protein phosphatase 1
Shc	0.035	Src homology collagen-like
Grb2	0.034	Growth factor receptor-bound protein 2
PP2A	0.033	Protein Phosphatase 2
MKP1	0.033	Mitogen-activated protein Kinase Phosphatase 1
Ng	0.033	Neurogranin
Src	0.032	Non-Receptor Tyrosine Kinase
Cbl	0.030	Casitas B-lineage Lymphoma
ERK	0.027	Mitogen-activated protein Kinase
PDE4	0.025	Phosphodiesterase 4
PKA	0.025	Protein Kinase A
NCX	0.022	Sodium Calcium Exchanger

SUPPLEMENTARY TABLES AND CAPTIONS

Figure 1 - Supplementary Table 1A: Reactions and rates constant involved in signaling pathway leading to Ras and Rap1 activation

Reaction equation	K_f (nM^{-1} Sec^{-1})	K_b (Sec^{-1})	K_{cat} (Sec^{-1})	Reference
Gby + Src ↔ Src_Gby	2.00E-04	1.00E-01		Estimated
Grb2 + Sos ↔ Grb2_Sos	2.50E-04	1.68E-02		Jain and Bhalla, 2014
Src_Gby +Shc ↔ pShc +Src_Gbg	8.00E-03	1.28E-01	3.20E-02	Estimated
pShc + Src_Grb2_Sos ↔ pShc_Grb2_Sos	5.00E+00	1.00E-01		Jain and Bhalla, 2014
pShc_Grb2_Sos + RasGDP ↔ pShc_Grb2_Sos + RasGTP	1.98E-02	8.00E-01	2.00E-01	Jain and Bhalla, 2014
pShc ↔ Shc	2.00E-01	0.00E+00		Jain and Bhalla, 2014
ppERK +pShc_Grb2_Sos↔ppERK +pShc_Grb2 + pSos	1.95E-02	4.00E+01	1.00E+01	Jain and Bhalla, 2014
psos↔sos	1.00E+00			Jain and Bhalla, 2014
CaMCa4 + Ras-GRF2 ↔ Ras-GRF2_CaMCa4	6.00E-02	9.24E-01		Jin et al., 2014
Ras-GRF2_CaMCa4 + RasGDP ↔ Ras-GRF2_CaMCa4 + RasGTP	1.98E-02	8.00E-01	2.00E-01	Jain and Bhalla, 2014; Jin et al., 2014
PKAc + Src ↔ pSrc + PKAc	2.04E+00	8.00E+01	2.00E+01	Jain and Bhalla, 2014
pSrc + Cbl ↔ pCbl + Src	4.00E-01	1.60E+02	4.00E+01	Jain and Bhalla, 2014
Crk_C3G + pCbl ↔ Crk_C3G_pCbl	1.00E-03	2.00E-01		Jain and Bhalla, 2014
pCbl ↔ Cbl	1.00E+02			Jain and Bhalla, 2014
pSrc ↔ Src	1.00E+02			Jain and Bhalla, 2014
Crk_C3G_pCbl + Rap1GDP ↔ Crk_C3G_pCbl + Rap1GTP	1.01E-02	8.00E-02	2.00E-02	Jain and Bhalla, 2014
Epac + cAMP ↔ Epac_cAMP	1.21E-04	1.45E-01		de Rooij et al., 2000; Luczak et al., 2017
Epac_cAMP + Rap1GDP ↔ Epac_cAMP + Rap1GTP	1.20E-03	9.60E-01	2.40E-01	Estimated
Rap1GTP+Rap1Gap ↔ Rap1GDP	2.00E-01	2.00E+02		Jain and Bhalla, 2014
RasGTP+ RasGap ↔ RasGDP	4.95E-02	4.00E+01		Jain and Bhalla, 2014

Figure 1 - Supplementary Table 1B: Reaction and rates constant involved in signaling pathway of SynGap. Rates were optimized from Oh et al., 2004 and Walkup IV et al., 2015 (https://github.com/neurord/neurord_fit/tree/master/syngap_ras)

Reaction equation	**K_f (nM^{-1} Sec^{-1})**	**K_b (Sec^{-1})**	**K_{cat} (Sec^{-1})**
CKpCaMCa4 + SynGAP ↔ pSynGAP + CKpCaMCa4	3.07E-01	5.87E+01	6.48E-01
Ras1GTP + SynGAP ↔ Ras1GDP + SynGAP	8.20E-04	8.20E-01	2.05E-01
Rap1GTP + SynGAP ↔ Rap1GDP + SynGAP	3.20E-03	3.20E+00	8.00E-01
RasGTP + pSynGAP ↔ RasGDP + pSynGAP	1.12E-03	1.11E+00	2.79E-01
Rap1GTP + pSynGAP ↔ Rap1GDP +pSynGAP	6.14E-03	6.14E+00	1.53E+00
pSynGAP ↔ SynGAP	1.00E+00	0.00E+00	
pSynGAP ↔ SynGap_dendrite	2.50E-02	2.50E-02	

Figure 1 - Supplementary Table 1C: Reactions and rates constant involved in core ERK signaling pathway

Reaction equation	K_f (nM^{-1} Sec^{-1})	K_b (Sec^{-1})	K_{cat} (Sec^{-1})	Reference
Rap1GTP + B-Raf ↔ B-Raf_Rap1GTP	6.00E-02	1.00E+00		Jain and Bhalla, 2014
Rap1GTP + Raf-1 ↔ RapGTP_Raf-1 + RasGTP	6.00E-03	5.00E-01		Jain and Bhalla, 2014
B-Raf_Rap1GTP + MEK ↔ pMEK + B-Raf_Rap1GTP	9.38E-03	1.20E+00	3.00E-01	Jain and Bhalla, 2014
B-Raf_Rap1GTP + pMEK ↔ ppMEK + B-Raf_Rap1GTP	9.38E-03	1.20E+00	3.00E-01	Jain and Bhalla, 2014
RasGTP + Raf1 ↔ Raf1_ RasGTP	6.00E-02	1.00E+00		Jain and Bhalla, 2014
2Raf1_ RasGTP ↔ dRaf1_ RasGTP	1.00E-02	5.00E-01		Estimated
RasGTP + bRaf ↔ bRaf_RasGTP	6.00E-03	5.00E-01		Jain and Bhalla, 2014
dRaf1_RasGTP + MEK ↔ pMEK + dRaf1_RasGTP	1.89E-02	2.40E+00	6.00E-01	Estimated
dRaf1_RasGTP + pMEK ↔ ppMEK + dRaf1_RasGTP	1.89E-02	2.40E+00	6.00E-01	Estimated
B-Raf _RasGTP + MEK ↔ pMEK + B-Raf _RasGTP	6.29E-03	8.00E-01	2.00E-01	Jain and Bhalla, 2014
B-Raf _RasGTP + pMEK ↔ ppMEK + B-Raf _RasGTP	6.29E-03	8.00E-01	2.00E-01	Jain and Bhalla, 2014
ppMEK + PP2A ↔ pMEK + PP2A	1.92E-03	2.40E+01	6.00E+00	Jain and Bhalla, 2014
ppMEK + PP2A ↔ MEK + PP2A	1.92E-03	2.40E+01	6.00E+00	Jain and Bhalla, 2014
ppMEK + ERK ↔ pERK + ppMEK	3.24E-02	1.20E+00	3.00E-01	Jain and Bhalla, 2014
ppMEK + ERK ↔ ppERK + ppMEK	3.24E-02	1.20E+00	3.00E-01	Jain and Bhalla, 2014
ppERK + MKP-1 ↔ pERK+ MKP-1	1.50E-01	1.60E+01	4.00E+00	Jain and Bhalla, 2014
pERK + MKP-1 ↔ ERK+ MKP-1	1.50E-01	1.60E+01	4.00E+00	Jain and Bhalla, 2014

Figure 1 - Supplementary Table 1D: Reaction and rates constant involved in signaling pathway of calcium to CaMKII. Where indicated, CaMKII was optimized using De Koninck and Schulman, 1998 (https://github.com/neurord/neurord_fit/tree/master/camkii)

Reaction equation	K_f (nM^{-1} Sec^{-1})	K_b (Sec^{-1})	K_{cat} (Sec^{-1})	Reference
Ca+ pmca ↔ pmca + Caext	5.00E-01	7.00E+00	3.50E+00	J□drzejewska-Szmek et al., 2017
Ca+ ncx ↔ ncx + Caext	1.68E-02	1.12E+01	5.60E+00	J□drzejewska-Szmek et al., 2017
Caext +Leak ↔ Ca + Leak	1.50E-03	1.10E+00	1.10E+00	J□drzejewska-Szmek et al., 2017
Ca + Calbin ↔ CalbinCa	2.80E-02	1.96E+01		J□drzejewska-Szmek et al., 2017
CB + Ca ↔ CBCa	2.00E-02	1.00E+03		Matthews et al., 2013; Matthews and Dietrich, 2015
Ng + CaM ↔ NgCaM	2.80E-02	3.60E+01		J□drzejewska-Szmek et al., 2017
CaM+2Ca ↔ CaMCa2C	6.00E-03	9.10E+00		J□drzejewska-Szmek et al., 2017
CaMCa2C + 2Ca ↔ CaMCa4	1.00E-01	1.00E+03		J□drzejewska-Szmek et al., 2017
CaM+2Ca ↔ CaMCa2N	1.00E-01	1.00E+03		J□drzejewska-Szmek et al., 2017
CaMCa2N + 2Ca ↔ CaMCa4	6.00E-03	9.10E+00		J□drzejewska-Szmek et al., 2017
CaMCa4+CK ↔ CKCaMCa4	1.00E-02	1.50E+00		J□drzejewska-Szmek et al., 2017
2CKCaMCa ↔ CKpCaMCa4+ CKCaMCa4	3.83E-07			optimized
3CKCaMCa ↔ CKpCaMCa4+ 2CKCaMCa4	3.56E-10			optimized
4CKCaMCa ↔ CKpCaMCa4+ 3CKCaMCa4	2.24E-13			optimized
2 CKpCaMCa4 + 2 CKCaMCa4 ↔ 3 CKpCaMCa4 + 1 CKCaMCa4	1.10E-15			optimized
2 CKpCaMCa4 + 2 CKCaMCa4 ↔ 3 CKpCaMCa4 + 1 CKCaMCa4	3.03E-10			optimized
2 CKpCaMCa4 + 2 CKCaMCa4 ↔ 3	2.39E-10			optimized

CKpCaMCa4 + 1 CKCaMCa4				
CKpCaMCa4 ↔ CKp + CaMCa4	8.00E-04	1.00E-02		J□drzejewska-Szmek et al., 2017
CKp+PP1 ↔ CK + PP1	4.00E-05	3.40E-01	8.60E-02	optimized
CKpCaMCa4 + PP1 ↔ CKCaMCa4 + PP1	4.00E-05	3.40E-01	8.60E-02	optimized
Ip35 + PP1 ↔ Ip35PP1	1.00E-03	1.10E-03		J□drzejewska-Szmek et al., 2017

Figure 1 - Supplementary Table 1E: Reactions and rates constant involved in signaling pathway leading from cAMP to PKA

Reaction equation	**K_f ($nM^{-1}Sec^{-1}$)**	**K_b (Sec^{-1})**	**K_{cat} (Sec^{-1})**	**Reference**
PKA + 2cAMP ↔ PKAcAMP2	2.16E-04	6.00E-02		J□drzejewska-Szmek et al., 2017
PKAcAMP2+2cAMP ↔ PKAcAMP4	3.50E-04	6.00E-01		J□drzejewska-Szmek et al., 2017
PKAcAMP4 ↔ PKAr + PKAc	2.40E-01	2.55E-02		J□drzejewska-Szmek et al., 2017
PDE2+cAMP ↔ PDE2cAMP	2.00E-05	5.00E-01		Blackwell et al., 2019
PDE2cAMP+cAMP ↔ PDE2cAMP2 +AMP	5.90E-03	5.00E-01	5.40E+00	Blackwell et al., 2019
PDE4+cAMP ↔ PDE4 +AMP	2.16E-02	6.90E+01	1.72E+01	J□drzejewska-Szmek et al., 2017

Figure 1 - Supplementary Table 2: Molecules total quantities

Molecules	Concentration (nM)
ERK	360
MEK	680
MKP1	40
PP2A	550
BRaf	300
Raf1	300
Rap1	400
Ras	600
PDE2	160
PDE4	100
PKA	1000
Epac	800
Src	20
Cbl	500
CRKC3G	500
Sos	100
RasGRF	400
SynGap	1000
rasGap	10
rap1Gap	12
Cam	28000
CK	20000
PP1	3600
Calbindin	160000
ncx	2000
pmca	500
CB (fixed buffer)	3000000
Ip35	500
Ng	21000
Leak	700
Grb2	1000

Figure 3- Supplementary Table 1: Regression analysis results for cAMP pathway. AIC: Akaike Information Criteria, lower values indicate better models. If Adjusted R^2 for linear is less than 0.9 then the best model is determined by AIC.

		Giβγ		**cAMP**	
		Dur	Conc	Dur	Conc
Adjusted R^2	Linear	0.832	0.827	0.951	0.937
	log	0.880	0.787	0.957	0.815
	Hill	0.922	0.913	0.969	0.964
AIC	Linear	-1.112	-8.266	-10.181	-52.828
	log	10.196	24.022	13.458	13.710
	Hill	-28.406	-38.033	-48.562	-48.911
Conclusion		**Non-Linear**	**Non-Linear**	**Linear**	**Linear**

Figure 4 - Supplementary Table 1: Regression analysis results for calcium pathway. AIC: Akaike Information Criteria, lower values indicate better models.

		Calcium	
		Dur	Conc
Adjusted R^2	Linear	0.486	0.675
	log	0.955	0.604
	Hill	0.970	0.989
AIC	Linear	166.225	99.958
	log	107.598	127.772
	Hill	-86.367	-101.415
Conclusion		**Non-Linear**	**Non-Linear**

Figure 8- Supplementary Table 1: Two-way ANCOVA (analysis of covariance) results of ppERK AUC versus stimulation characteristics (ITI) and type (combination versus summation) as factors (N=5 in each group).

	cAMP+Giβγ+Calcium		
	0.5 μM Ca	***18 % PP1***	***50 % PP1***
F (2,47)	43.56	28.28	3.99
P (ITI)	**<0.0001**	**<0.0001**	**0.023**
T (ITI)	9.11	6.43	2.36
P (type)	0.05	**<0.0001**	0.13
T (type)	-2.04	-3.90	-1.56
Conclusion	Significant for **stim** only	Significant for **both** type and stim	Significant for **stim** only

REFERENCES for supplementary materials

1. Blackwell, K.T., Salinas, A.G., Tewatia, P., English, B., Kotaleski, J.H., Lovinger, D.M., 2019. Molecular mechanisms underlying striatal synaptic plasticity: relevance to chronic alcohol consumption and seeking. Eur. J. Neurosci. 49, 768–783.

2. De Koninck, P., Schulman, H., 1998. Sensitivity of CaM Kinase II to the Frequency of Ca^{2+} Oscillations. Science 279, 227–230.

3. de Rooij, J., Rehmann, H., van Triest, M., Cool, R.H., Wittinghofer, A., Bos, J.L., 2000. Mechanism of Regulation of the Epac Family of cAMP-dependent RapGEFs. J. Biol. Chem. 275, 20829–20836.

4. Jain, P., Bhalla, U.S., 2014. Transcription Control Pathways Decode Patterned Synaptic Inputs into Diverse mRNA Expression Profiles. PLoS ONE 9, e95154.

5. J□drzejewska-Szmek, J., Luczak, V., Abel, T., Blackwell, K.T., 2017. β-adrenergic signaling broadly contributes to LTP induction. PLOS Comput. Biol. 13, e1005657.

6. Jin, S.-X., Bartolome, C., Arai, J.A., Hoffman, L., Uzturk, B.G., Kumar-Singh, R., Waxham, M.N., Feig, L.A., 2014. Domain Contributions to Signaling Specificity Differences Between Ras-Guanine Nucleotide Releasing Factor (Ras-GRF) 1 and Ras-GRF2. J. Biol. Chem. 289, 16551–16564.

7. Luczak, V., Blackwell, K.T., Abel, T., Girault, J.-A., Gervasi, N., 2017. Dendritic diameter influences the rate and magnitude of hippocampal cAMP and PKA transients during β-adrenergic receptor activation. Neurobiol. Learn. Mem. 138, 10–20.

8. Matthews, E.A., Dietrich, D., 2015. Buffer mobility and the regulation of neuronal calcium domains. Front. Cell. Neurosci. 9, 48.

9. Matthews, E.A., Schoch, S., Dietrich, D., 2013. Tuning local calcium availability: cell-type-specific immobile calcium buffer capacity in hippocampal neurons. J. Neurosci. Off. J. Soc. Neurosci. 33, 14431–14445.

10. Oh, J.S., Manzerra, P., Kennedy, M.B., 2004. Regulation of the Neuron-specific Ras GTPase-activating Protein, synGAP, by Calcium /Calmodulin-dependent Protein Kinase II. J. Biol. Chem. 279, 17980–17988.

11. Walkup IV, W.G., Washburn, L., Sweredoski, M.J., Carlisle, H.J., Graham, R.L., Hess, S., Kennedy, M.B., 2015. Phosphorylation of Synaptic GTPase-activating Protein (synGAP) by Ca^{2+} /Calmodulin-dependent Protein Kinase II (CaMKII) and Cyclin-dependent Kinase 5 (CDK5) Alters the Ratio of Its GAP Activity toward Ras and Rap GTPases. J. Biol. Chem. 290, 4908–4927.

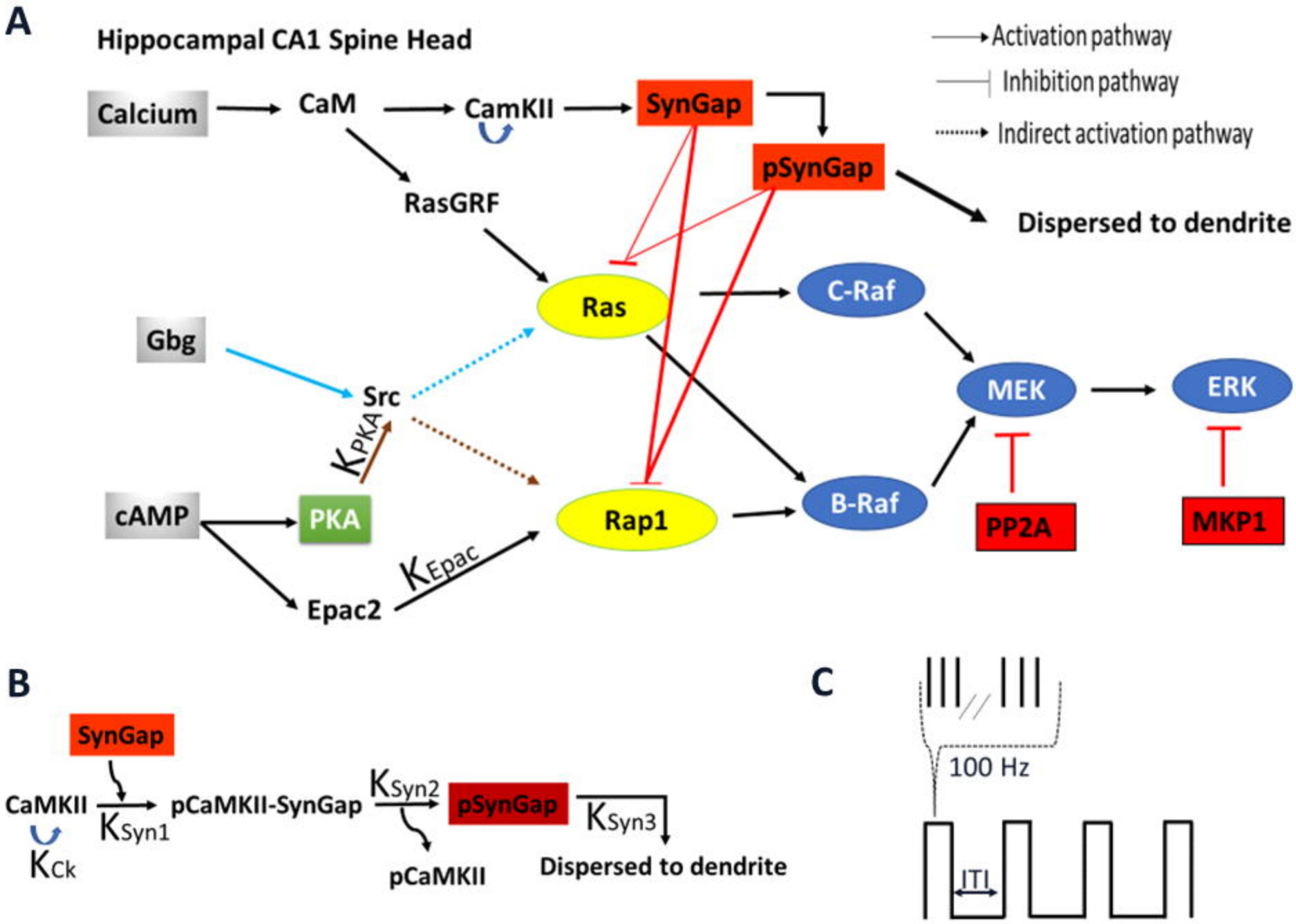
A
Hippocampal CA1 Spine Head
Activation pathway
Inhibition pathway
Indirect activation pathway
Calcium
CaM
CamKII
SynGap
pSynGap
RasGRF
Dispersed to dendrite
Ras
C-Raf
Gbg
Src
MEK
ERK
KPKA
cAMP
PKA
Rap1
B-Raf
PP2A
MKP1
KEpac
Epac2
B
SynGap
CaMKII
KSyn1
pCaMKII-SynGap
KSyn2
pSynGap
KSyn3
KCk
pCaMKII
Dispersed to dendrite
C
100 Hz
ITI

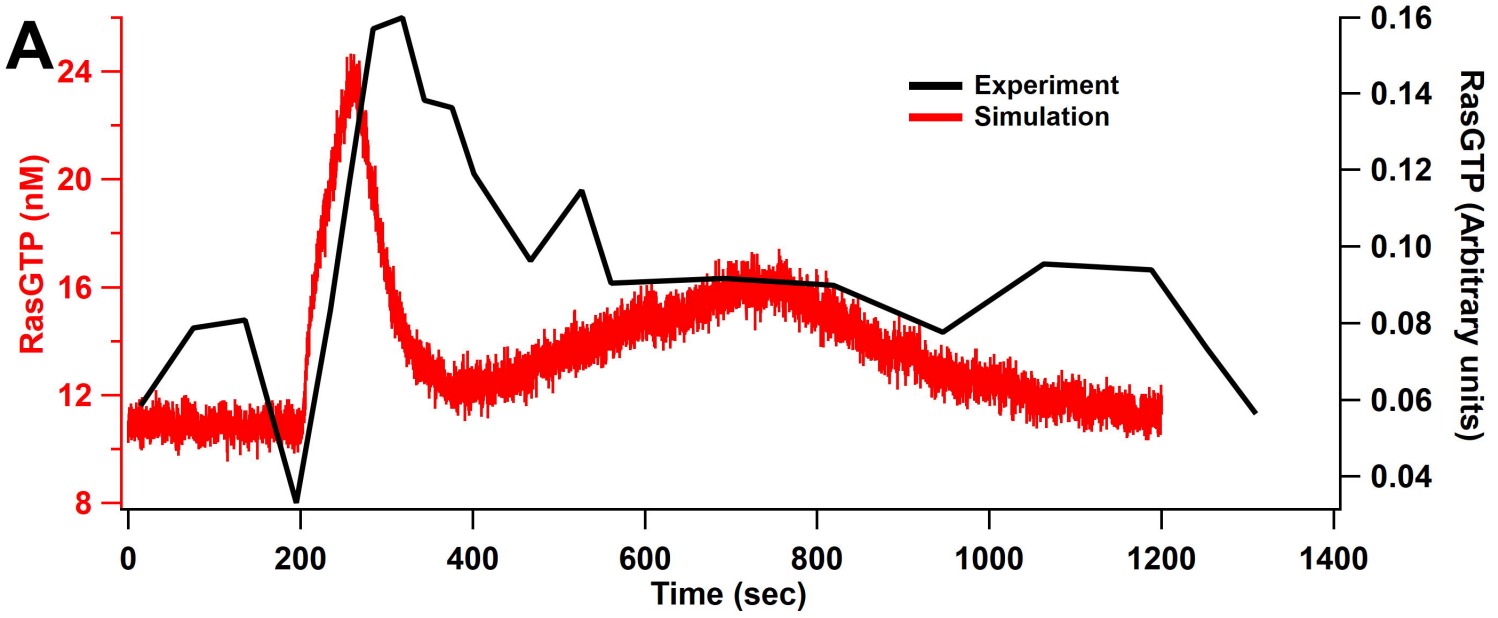
A
RasGTP (nM)
24
20
16
12
8
RasGTP (Arbitrary units)
0.16
0.14
0.12
0.10
0.08
0.06
0.04
Experiment
Simulation
0
200
400
600
800
1000
1200
1400
Time (sec)

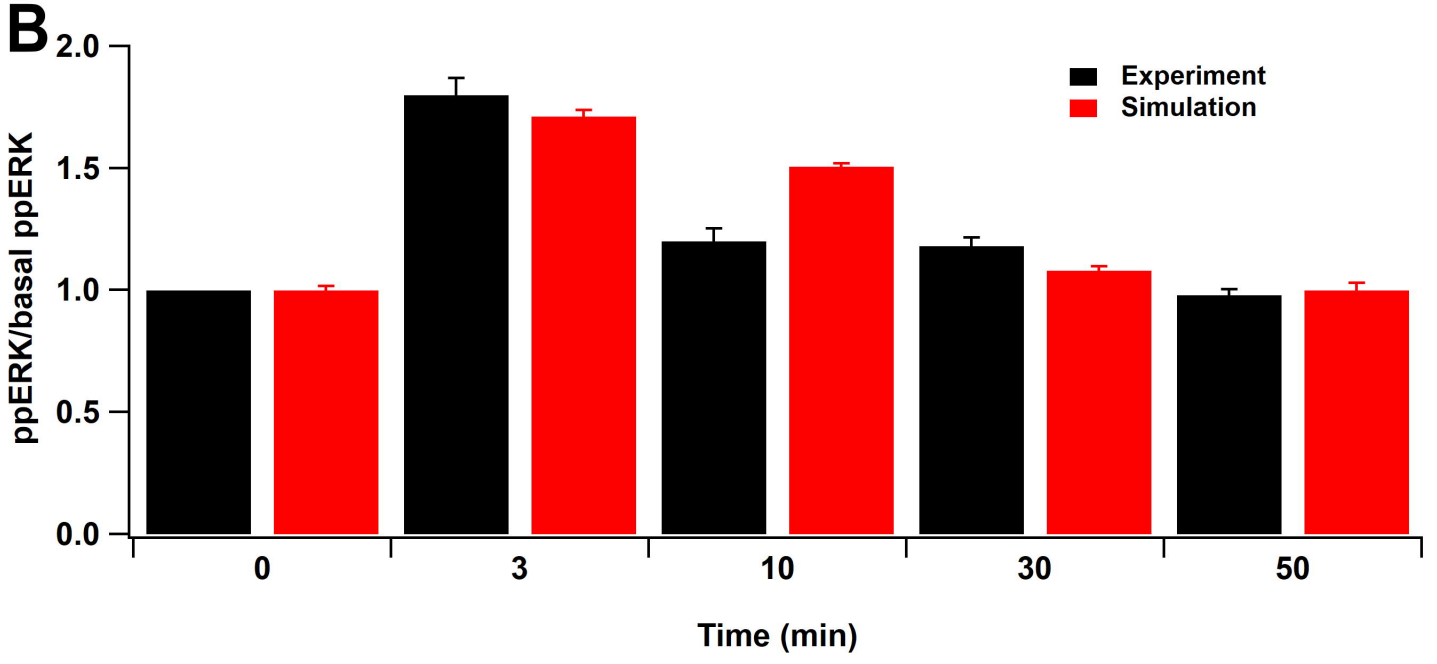
B
ppERK/basal ppERK
2.0
1.5
1.0
0.5
0.0
Experiment
Simulation
0
3
10
30
50
Time (min)

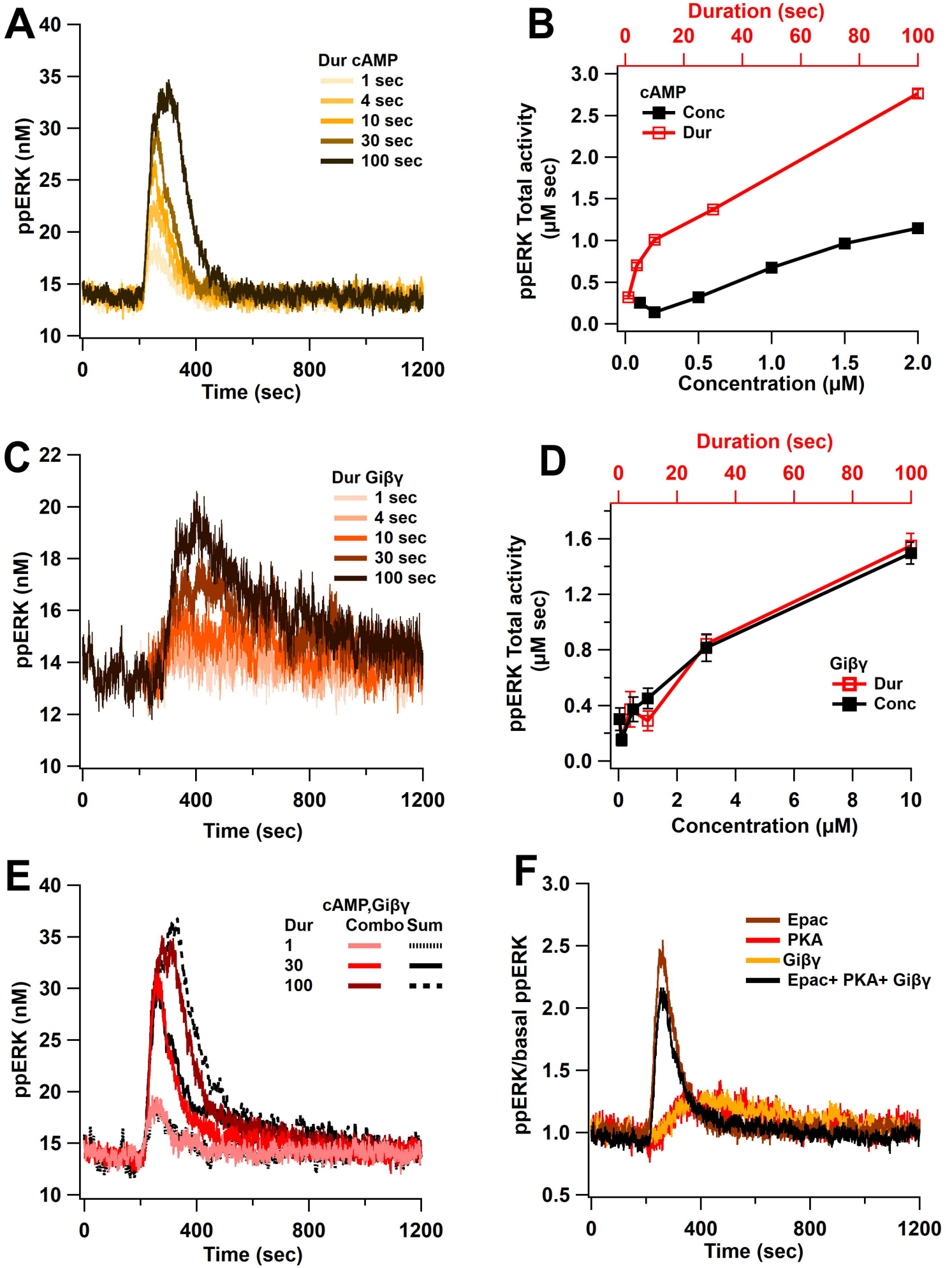
A
ppERK (nM)
Time (sec)
Dur cAMP
1 sec
4 sec
10 sec
30 sec
100 sec
B
Duration (sec)
ppERK Total activity (μM sec)
Concentration (μM)
cAMP
Conc
Dur
C
ppERK (nM)
Time (sec)
Dur Giβγ
1 sec
4 sec
10 sec
30 sec
100 sec
D
Duration (sec)
ppERK Total activity (μM sec)
Concentration (μM)
Giβγ
Dur
Conc
E
ppERK (nM)
Time (sec)
cAMP,Giβγ
Dur
Combo
Sum
1
30
100
F
ppERK/basal ppERK
Time (sec)
Epac
PKA
Giβγ
Epac+ PKA+ Giβγ

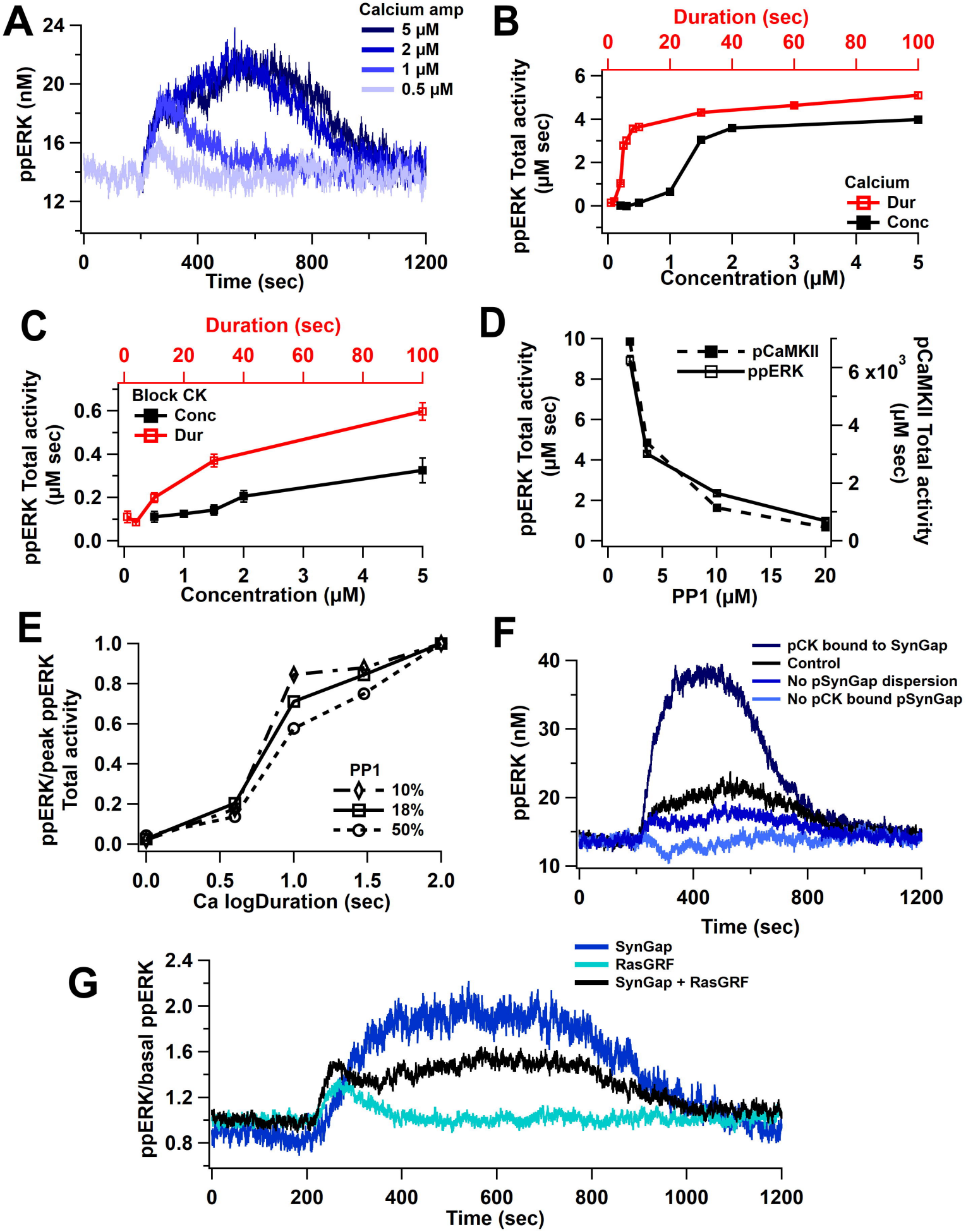
A
Calcium amp
5 μM
2 μM
1 μM
0.5 μM
ppERK (nM)
Time (sec)
B
Duration (sec)
ppERK Total activity (μM sec)
Calcium
Dur
Conc
Concentration (μM)
C
Duration (sec)
Block CK
Conc
Dur
ppERK Total activity (μM sec)
Concentration (μM)
D
pCaMKII
ppERK
ppERK Total activity (μM sec)
pCaMKII Total activity (μM sec)
PP1 (μM)
E
ppERK/peak ppERK Total activity
PP1
10%
18%
50%
Ca logDuration (sec)
F
pCK bound to SynGap
Control
No pSynGap dispersion
No pCK bound pSynGap
ppERK (nM)
Time (sec)
G
SynGap
RasGRF
SynGap + RasGRF
ppERK/basal ppERK
Time (sec)

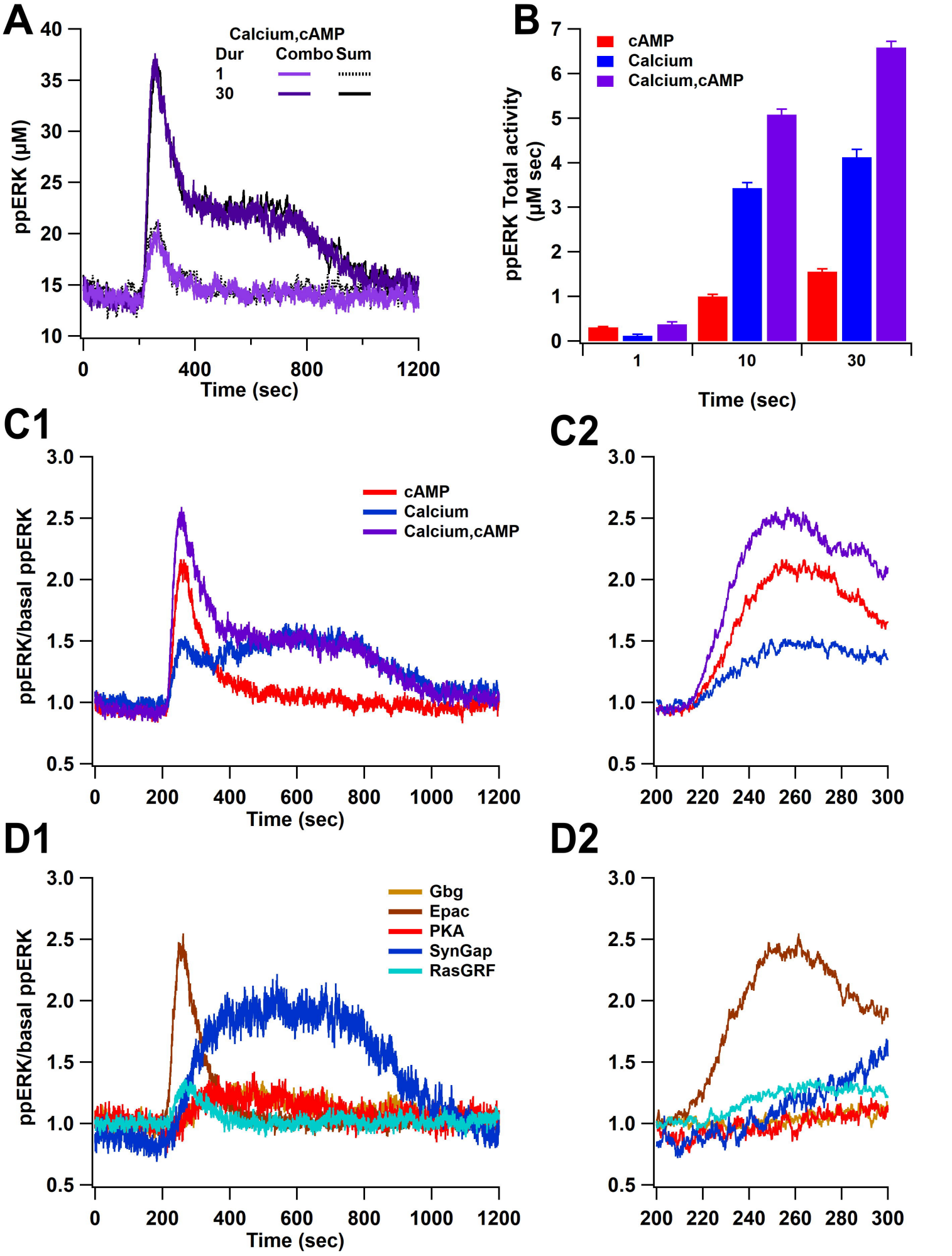
A
Calcium,cAMP
Dur
Combo
Sum
1
30
ppERK (μM)
Time (sec)
B
cAMP
Calcium
Calcium,cAMP
ppERK Total activity (μM sec)
1
10
30
Time (sec)
C1
C2
cAMP
Calcium
Calcium,cAMP
ppERK/basal ppERK
Time (sec)
D1
D2
Gbg
Epac
PKA
SynGap
RasGRF
ppERK/basal ppERK
Time (sec)

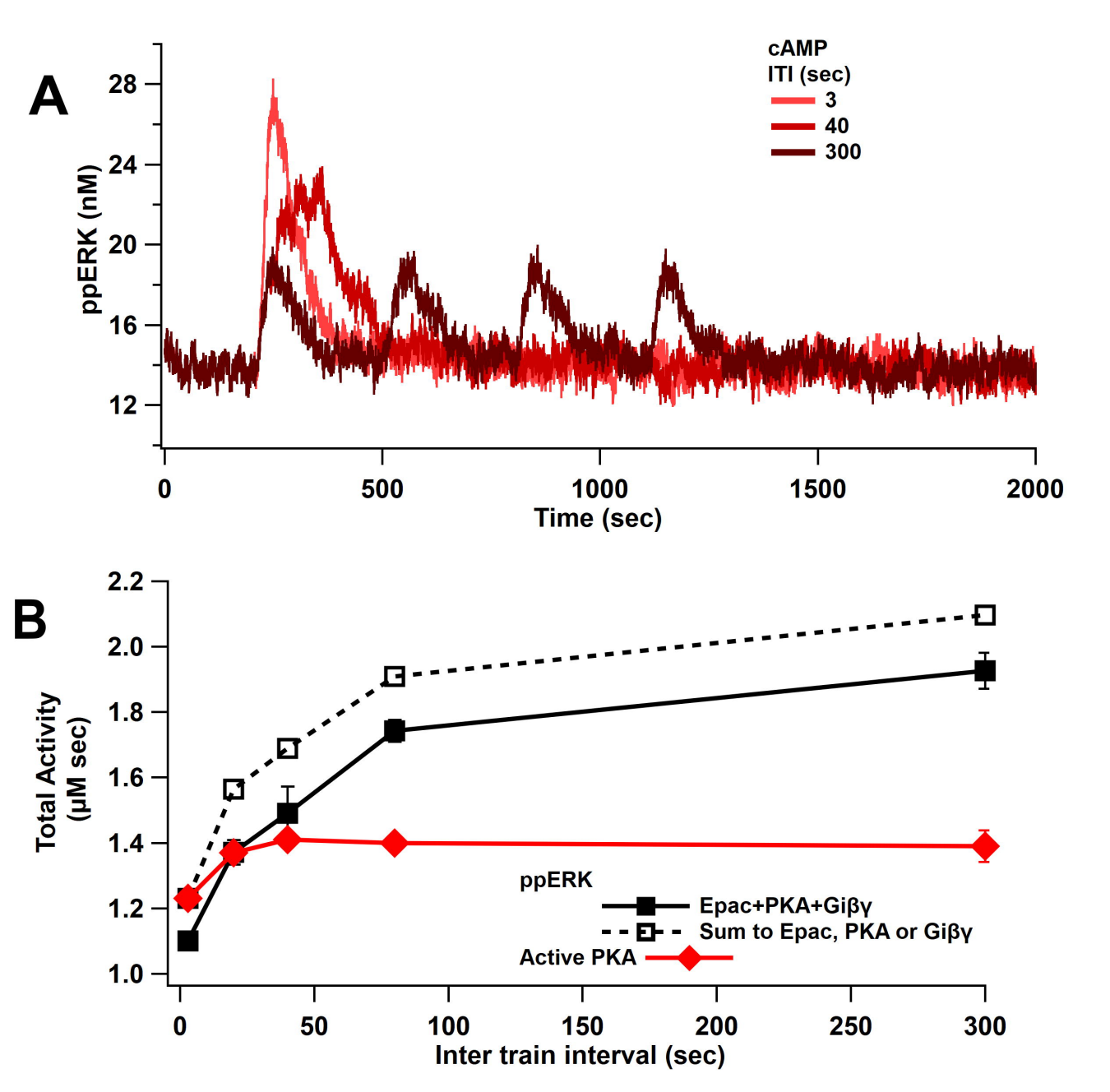
A
cAMP
ITI (sec)
3
40
300
ppERK (nM)
28
24
20
16
12
0
500
1000
1500
2000
Time (sec)
B
Total Activity
(μM sec)
2.2
2.0
1.8
1.6
1.4
1.2
1.0
ppERK
Epac+PKA+Giβγ
Sum to Epac, PKA or Giβγ
Active PKA
0
50
100
150
200
250
300
Inter train interval (sec)

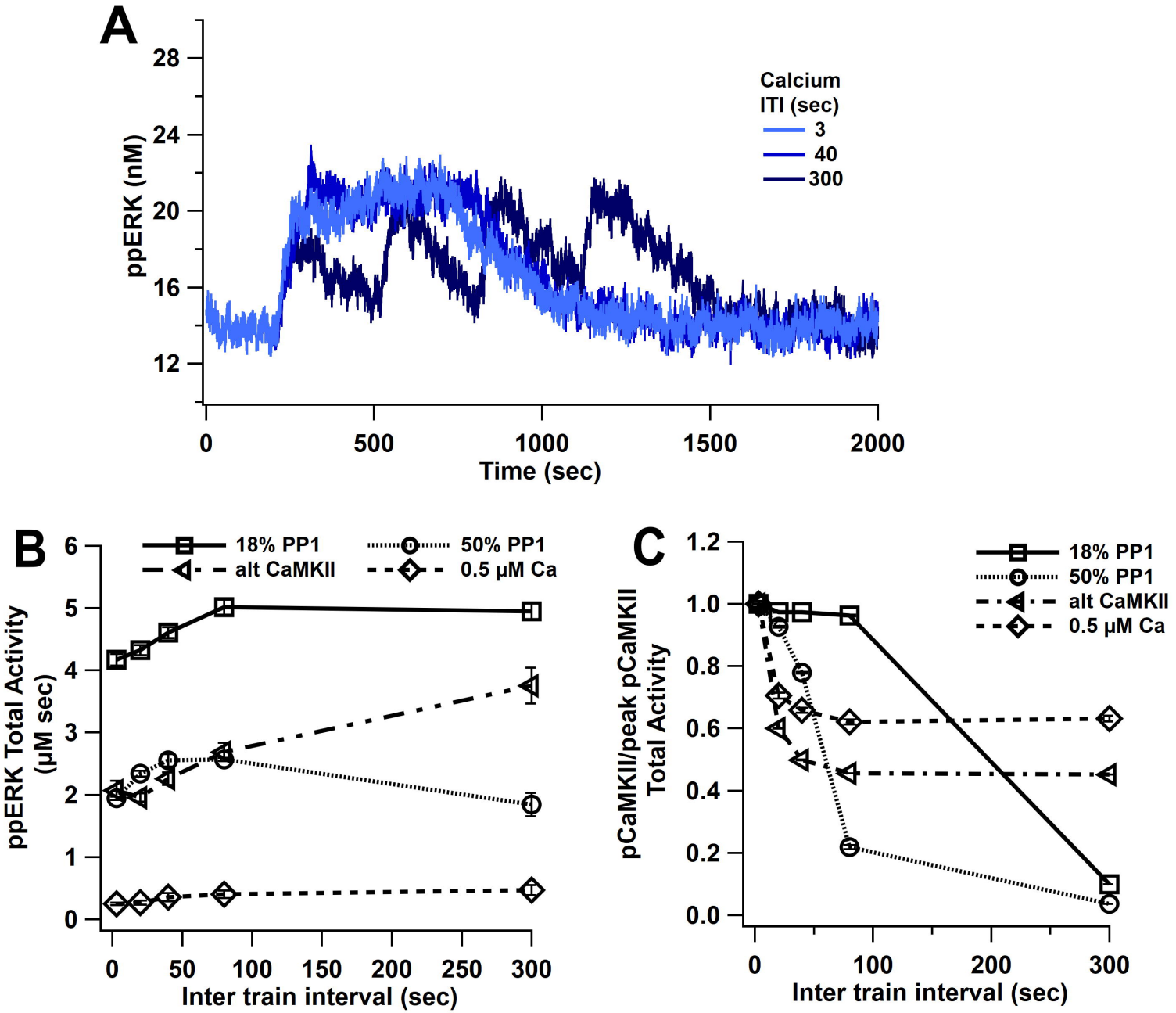
A
ppERK (nM)
28
24
20
16
12
0
500
1000
1500
2000
Time (sec)
Calcium
ITI (sec)
3
40
300
B
ppERK Total Activity
(μM sec)
6
5
4
3
2
1
0
0
50
100
150
200
250
300
Inter train interval (sec)
18% PP1
50% PP1
alt CaMKII
0.5 μM Ca
C
pCaMKII/peak pCaMKII
Total Activity
1.2
1.0
0.8
0.6
0.4
0.2
0.0
0
100
200
300
Inter train interval (sec)
18% PP1
50% PP1
alt CaMKII
0.5 μM Ca

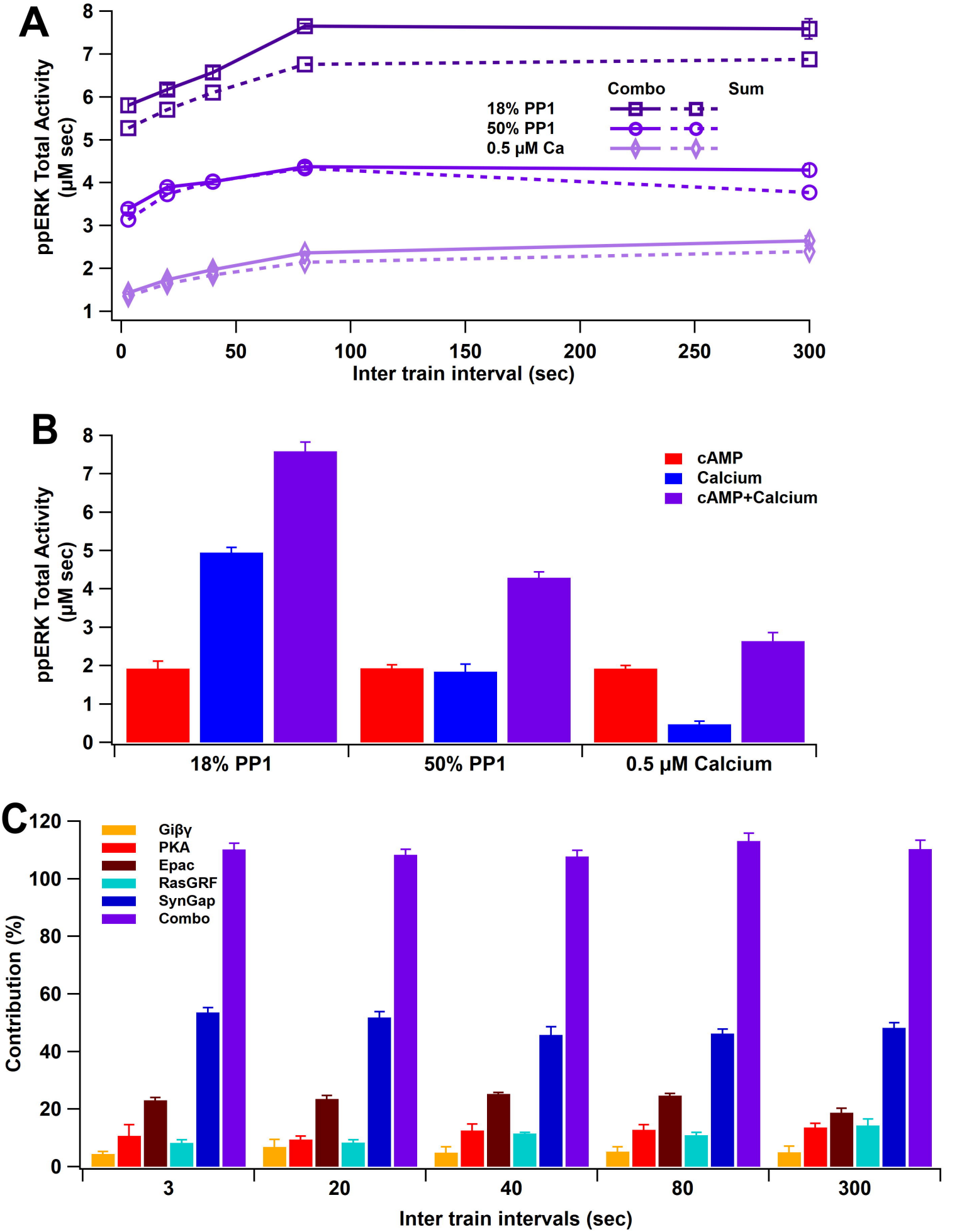
A
ppERK Total Activity (µM sec)
Inter train interval (sec)
Combo
Sum
18% PP1
50% PP1
0.5 µM Ca
B
ppERK Total Activity (µM sec)
cAMP
Calcium
cAMP+Calcium
18% PP1
50% PP1
0.5 µM Calcium
C
Contribution (%)
Giβγ
PKA
Epac
RasGRF
SynGap
Combo
Inter train intervals (sec)

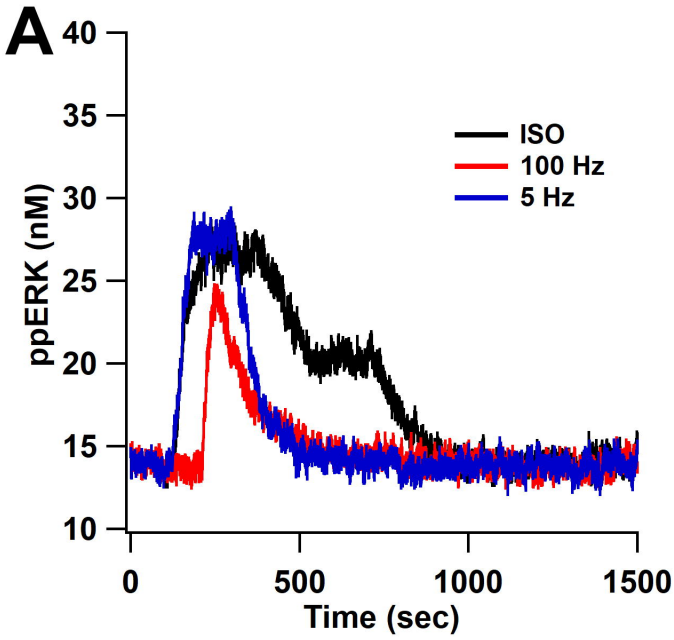
A
40
35
30
25
20
15
10
ppERK (nM)
ISO
100 Hz
5 Hz
0
500
1000
1500
Time (sec)

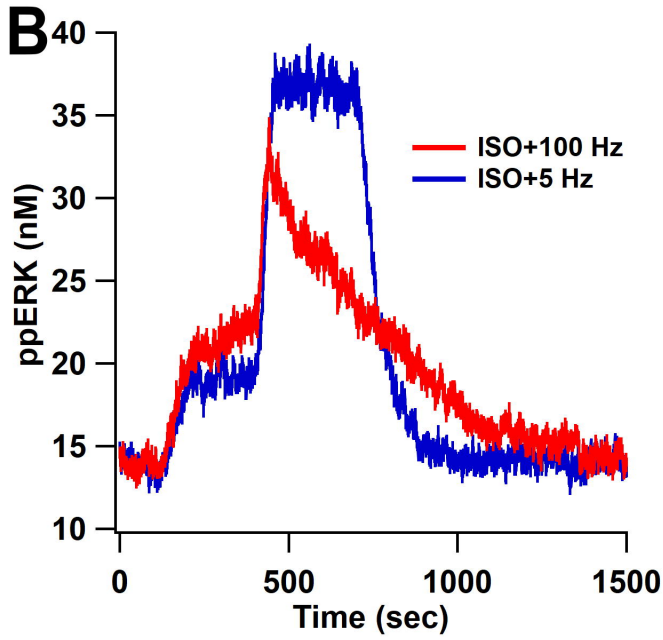
B
40
35
30
25
20
15
10
ppERK (nM)
ISO+100 Hz
ISO+5 Hz
0
500
1000
1500
Time (sec)

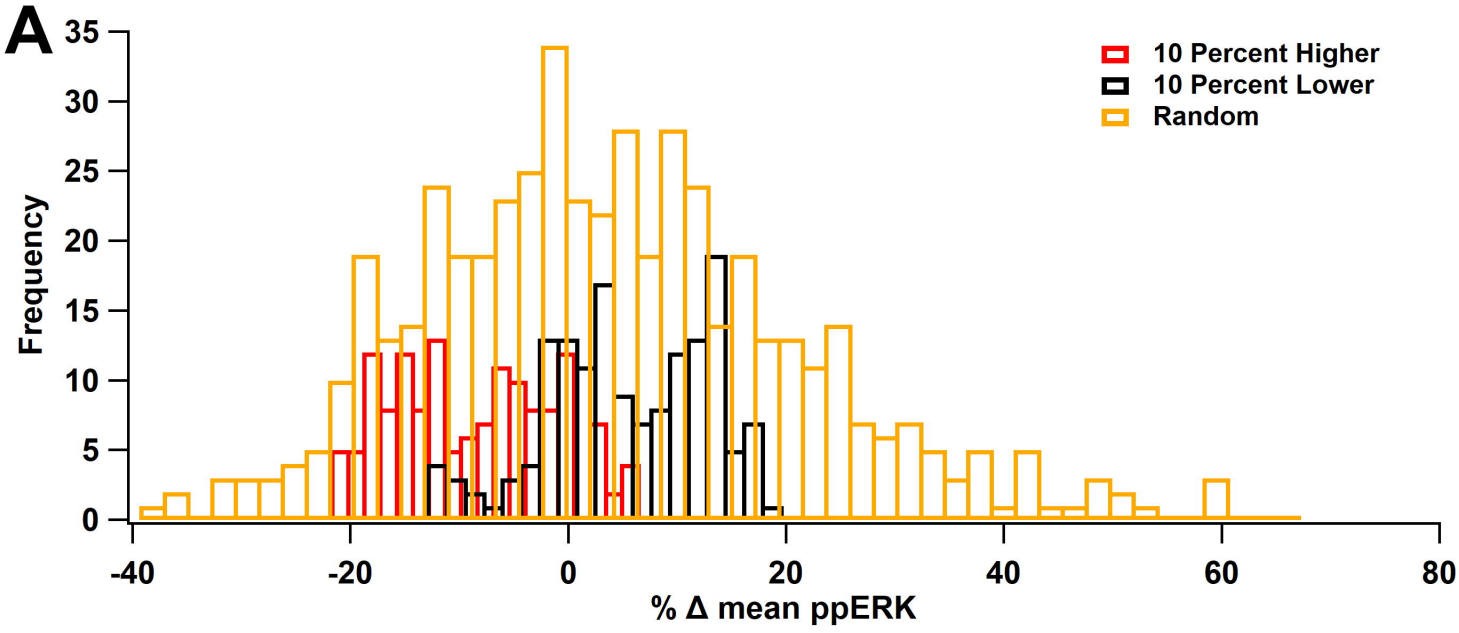
A
10 Percent Higher
10 Percent Lower
Random
Frequency
0
5
10
15
20
25
30
35
-40
-20
0
20
40
60
80
% Δ mean ppERK

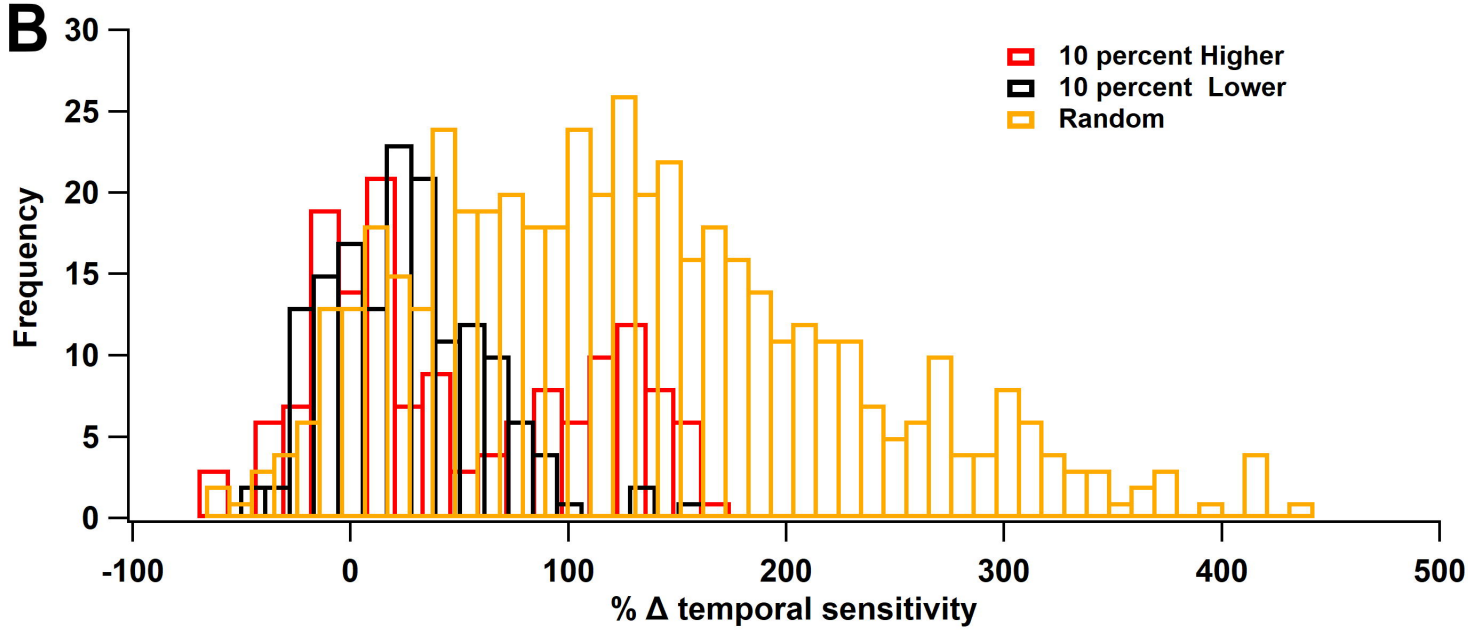
B
10 percent Higher
10 percent Lower
Random
Frequency
0
5
10
15
20
25
30
-100
0
100
200
300
400
500
% Δ temporal sensitivity